

**Fig. 3.** (A) Relative body weights of dams immunized with rAd-gB (continuous lines), with rAd-LacZ (dashed lines), and with PBS (gray) followed by GPCMV challenge (arrow) are shown by using the body weight of each animal at the time of the GPCMV challenge (arrows) as a 100% control. Comparison of weights of the placentas (B) and fetuses (C) from dams without any treatment (open circles) and from dams immunized with rAd-gB (closed circles) or rAd-LacZ (gray circles). Each circle indicates one placenta or fetus. Means and SDs are shown. An asterisk means  $p < 0.01$ .

became detectable by 3-weeks after infection irrespective of the gestational age of the dams (data not shown). Based on this observation, we designed the experimental schedule as follows: guinea pigs were inoculated with  $10^{10}$  TUs of Ad-LacZ or Ad-gB at 1-week of gestation, infected subcutaneously with  $10^6$  IUs of GPCMV at 4-weeks of gestation, and then sacrificed at 7-weeks of gestation. Although there was no difference in weight between the placentas from the gB- and LacZ-immunized dams, there was a significant difference in weight between the fetuses from the gB-immunized dams and those from the LacZ-immunized dams (Fig. 3). Taking the mean and standard deviation (SD) of the weight of the fetuses from untreated dams as the standard, we found that 42% of the fetuses from the LacZ-immunized dams exhibited IUGR, which was defined as a fetal weight less than the mean-1.5SD, whereas none of those from the gB-immunized dams did. Viral DNAs were detected by PCR in 75% and 13% of the fetuses from the LacZ- and gB-immunized dams, respectively (Fig. 4A). Two out of 16 fetuses from the gB-immunized dams (#A-1 and #B-5) were GPCMV positive. GPCMV

DNAs were detected in most of their organs, and the viral loads in each organ were comparable to those from the LacZ-immunized dams (Fig. 4B).

3.3. Serological observations after challenge

Anti-gB antibody titers in the fetuses from the gB-immunized dams were similar to those of the dams (Fig. 5A). This was also true for the avidity indices against anti-gB IgG (Fig. 5B). As compared with the dams inoculated with rAd-LacZ, the anti-gB antibody titers and the avidity indices were significantly higher in the dams inoculated with rAd-gB, suggesting the presence of efficient pre-existing immunity in the dams immunized with rAd-gB.

No differences in weight in the placentas or fetuses, in the anti-gB IgG levels, or in the avidity indices (data not shown) were observed among the littermates of the gB-immunized dam A (#1–#4) as well as among those of dam B (#5–#8), suggesting

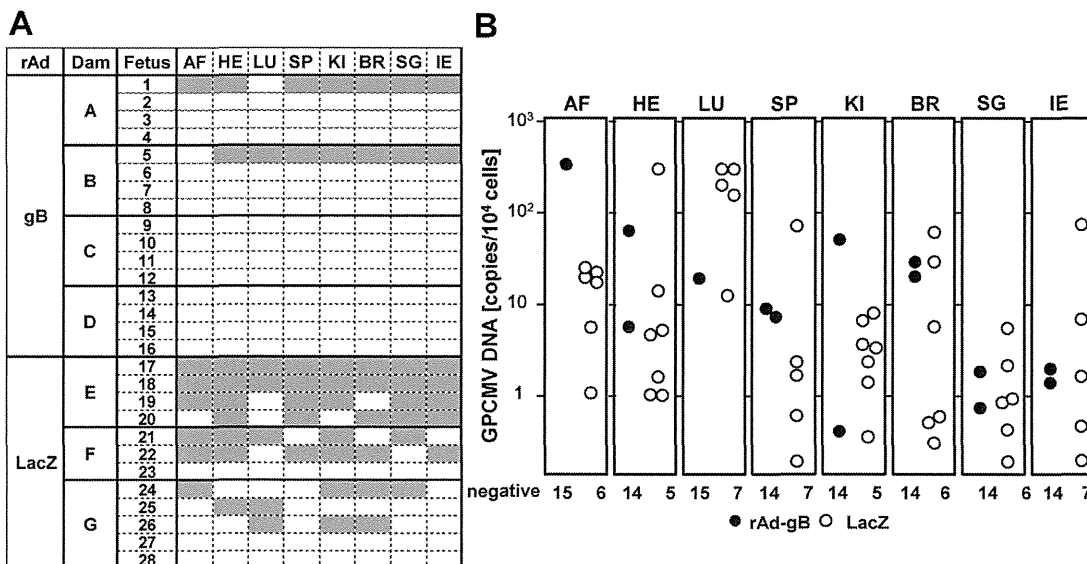


**Fig. 4.** GPCMV DNA detected in the organs of fetuses from dams immunized rAd-gB or -LacZ. (A) Shaded boxes indicate the presence of GPCMV DNA. (B) Viral loads (GPCMV DNA copies per  $10^4$  cells) of the organs from the fetuses are plotted. AF: amnion fluid, HE: heart, LU: lung, SP: spleen, KI: kidney, BR: brain, SG: salivary gland, and IE: inner ear.

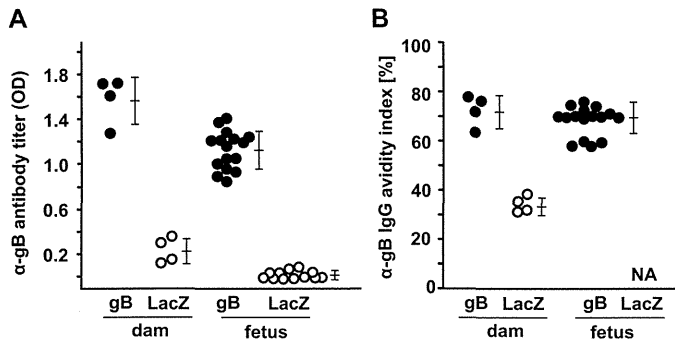


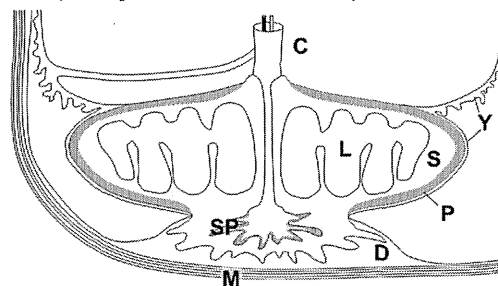
**Fig. 5.** Comparison of the anti-gB IgG titers and avidity indices against gB in sera obtained from dams immunized with rAd-gB (closed circles) or rAd-LacZ (open circles) and in sera from the fetuses. Each circle indicates one dam or fetus. Means and SDs are shown.

that gB-immunization protects the fetuses from IUGR irrespective of congenital infection and that the presence of anti-gB antibodies in the fetuses is not a sufficient determinant for protection from congenital infection.

**3.4. Localization of GPCMV antigens in the placenta from gB-immunized dams**

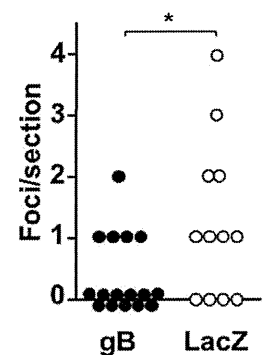
Immunohistochemical analysis using the anti-GPCMV monoclonal antibody g-1, which recognizes a 50-kDa viral protein expressed during the early phase of infection, showed that viral antigens were present focally in the placentas. In experiment A, in which the placenta specimens indicated in Figs. 3–5 were analyzed, 5 out of the 16 placentas from the gB-immunized dams were CMV positive, while 8 out of the 12 placentas from the LacZ-immunized dams were positive (Fig. 6B). The use of polyclonal antibodies against the IE2 protein gave similar results (data not shown). Taking into account the number of foci per slice, we found that more viral antigens were detected in the placentas of the LacZ-immunized dams ( $p < 0.05$ ). However, as the difference was small, an additional set of dams were analyzed in the same way (experiment B), with similar results obtained in those animals. A comparison of CMV-positive rates in the placentas from gB- and LacZ-immunized dams in the combined results from experiments A and B revealed a statistical significance ( $p < 0.05$ ), indicating the gB-immunization reduced CMV infection in the placentas. In the placentas from the dams immunized with rAd-LacZ, viral antigens

**A (adapted from ref.27)**



**B**

rAd	CMV	Exp. A	Exp. B	total	p
gB	+	5	3	8	<0.05
	-	11	4	15	
LacZ	+	8	4	12	<0.05
	-	4	2	6	



**C**

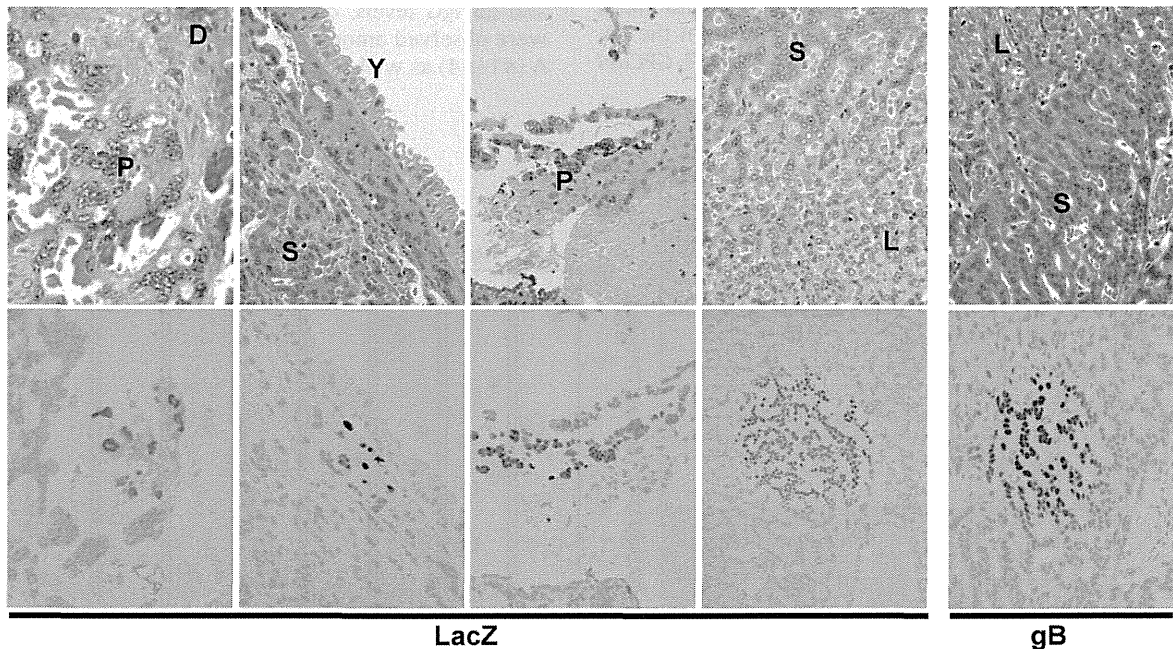


**Fig. 6.** Detection of viral antigens in the placentas. (A) Schematic presentation of the placental structure of guinea pigs (adapted from Ref. [27]). C: cord, M: myometrium, D: decidua, SP: subplacenta, Y: visceral yolk sac, P: parietal yolk sac, S: spongiotrophoblast layer, and L: labyrinth. (B) Numbers of CMV-positive foci in the placentas from rAd-gB- and rAd-LacZ-immunized dams. Two experiments, A and B, were performed. In the experiments (Exp.) A and B, the placenta specimens indicated in Figs. 3–5 and those obtained from an additional set of immunized dams were analyzed. A comparison of the number of foci per section in the placentas from dams immunized with rAd-gB (closed circles) or rAd-LacZ (open circles) in Exp. A is shown. An asterisk represents  $p < 0.05$ . (C) Localization of viral antigens in the placenta. HE staining (upper panels) and immunohistochemistry with anti-GPCMV antibody g-1 (lower panels) are shown.

were mainly detected in the spongiotrophoblast layer, occasionally in trophoblast giant cells in the parietal yolk sac, and only sporadically in the visceral yolk sac (Fig. 6C). No destruction of the spongy structure or inflammation was observed in the spongiotrophoblast layer. In contrast, some structural destruction and inclusion bodies were occasionally observed in the yolk sac. In the gB-immunized dams, viral antigens were detected only in the spongiotrophoblast layer. However, there was no apparent difference in the size of the CMV-positive foci in the spongiotrophoblast layer between the rAd-gB- and rAd-LacZ-immunized groups.

#### 4. Discussion

Guinea pig models have been used for many years in an attempt to clarify the pathogenesis of congenital CMV infection. However, most prior studies using the guinea pig model for vaccine studies have focused on infection in pups. Since guinea pigs consume the placentas after delivery, there is little information on how CMV spreads in the placentas and then into the fetuses and on how gB vaccination prevents viral spread to and in the placenta. In addition, most prior studies used sera obtained from GPCMV-infected animals; in other words, sera in which active infection cannot be distinguished from abortive infection. Thus, our study is unique in undertaking the precise analysis of viral spread in placentas using a well-characterized monoclonal antibody. The most important findings in this study are as follows: (i) immunization of dams with gB reduced the level of viral antigens in the placentas slightly, but significantly, (ii) this slight reduction in viral load resulted in marked differences in the rates of IUGR (42% vs. 0%) and congenital infection (75% vs. 13%), (iii) gB immunization did not inhibit focal virus growth in the placentas, and (iv) the presence of anti-gB antibodies in the fetuses did not protect against viral spread in the fetuses.

Schleiss et al. demonstrated that preconceptional immunization with purified gB in combination with Freund's adjuvant reduced both pup mortality to 14% and CMV-infection in liveborn pups to 22% vs. 76% and 50%, respectively, in the unvaccinated group [13], and that a DNA vaccine expressing gB did not improve pup mortality but reduced the rate of viral transmission by half [14]. Similarly, immunization with GPCMV glycoproteins reduced pup mortality to 14% vs. 56% in the unvaccinated group [20]. The absence of any difference in the birth weight of pups born from dams with and without immunization is thought to be due to their comparison of the weights of only liveborn pups. The rate of congenital infection and the efficacy of gB immunization in our study were generally consistent with the results observed in those studies.

GPCMV infection in the placenta occurred focally in the spongiotrophoblast layer at a relatively low frequency, suggesting cell-to-cell spread of the virus in the placenta. This is consistent with previous studies that reported localization of viral antigens at the transitional zone between the capillarized labyrinth and the noncapillarized interlobium, presumably the spongiotrophoblast layer, with GPCMV-related lesions [15]. In humans, HCMV proteins have also been detected in focal areas in the term placenta [21]. The fact that gB immunization did not change the focal spread of GPCMV in the spongiotrophoblast layer, but reduced the number of foci, suggests that anti-gB antibodies are not effective against this form of viral spread in the placenta and that anti-gB antibodies mainly protect against infection at the interface of the placenta rather than inside the placenta or from the placenta to the fetus.

Recent studies on HCMV have demonstrated that human sera obtained from individuals naturally infected, but not from those immunized with the gB subunit vaccine or with the attenuated strain Towne, contain strong neutralizing activities against infection to endothelial and epithelial cells [22]. HCMV entry into endothelial cells can be inhibited with antibodies against UL128,

UL130 and UL131A [23]. Since the major cell types comprising the placenta are cytotrophoblasts and syncytiotrophoblasts, both of which possess similarities to epithelial cells, and vascular endothelial cells, it is plausible that neutralizing antibodies against gB cannot efficiently inhibit viral spread in the placenta. The neonatal Fc receptor mediated-transcytosis of CMV virions has been proposed as one possible mechanism for viral dissemination in the placenta, thus highlighting the importance of the quality and quantity of CMV-specific neutralizing antibodies to the prevention of viral transmission to the fetus [24]. It would be interesting to see whether immunization with the gH/gL/UL128/UL130/UL131A pentamer complex could protect the placenta against CMV infection. Although we tried to induce antibodies against GPCMV GP131, the HCMV UL130 homolog, by using the same rAd system, we could not induce a high level of anti-GP131 antibodies (data not shown).

The significant rate of IUGR observed in spite of the limited viral activity in the placenta suggests that infection induces secondary effects on placental functions. It would be important to identify which of the cellular genes are affected by CMV infection in the placenta. A recent study on amnion fluid specimens from pregnant women with congenital HCMV infection demonstrated that HCMV infection during pregnancy was associated with a shift in cytokine expression toward a proinflammatory state [25]. Pathological analyses on the placentas from women with congenital infection indicated that vascular endothelial growth factor (VEGF) and its receptor, fms-like tyrosine kinase 1 (Flt1), were up-regulated, and the amniotic fluid contained elevated levels of soluble Flt1 (sFlt1), an antiangiogenic protein, relative to placental growth factor. Hyperimmune globulin treatment reduced both VEGF and Flt1 expression as well as the sFlt1 levels [26]. Microarray analyses of cellular gene expression in the placentas of GPCMV-infected guinea pigs are currently under way.

In conclusion, this study demonstrated that a slight reduction in placental infection by immunization with gB can result in a significant prevention of IUGR and congenital infection, and that gB immunization may not be effective in reducing viral spread in the placenta.

#### Acknowledgements

We thank Yoshiko Fukui and Mihoko Tsuda for their technical assistance and Yoshihiro Tsutsui for the monoclonal antibody g-1. This work was supported by the following grants: Grant on Research on Health Sciences focusing on Drug Innovation (SHC4401) from Japanese Human Science Foundation to NI and HK, and Grants-in-Aid for Scientific Research C and for Young Scientists B from the Japan Society for the Promotion of Science to NI and SY, respectively.

*Conflict of interest statement:* No authors have any conflict of interest.

#### References

- [1] Koyano S, Inoue N, Nagamori T, Yan H, Asanuma H, Yagyu K, et al. Dried umbilical cords in the retrospective diagnosis of congenital cytomegalovirus infection as a cause of developmental delays. *Clin Infect Dis* 2009;48:e93–5.
- [2] Ogawa H, Suzutani T, Baba Y, Koyano S, Nozawa N, Ishibashi K, et al. Etiology of severe sensorineural hearing loss in children: independent impact of congenital cytomegalovirus infection and GJB2 mutations. *J Infect Dis* 2007;195:782–8.
- [3] Pass RF. Cytomegalovirus. In: Knipe DM, Howley PM, editors. *Fields virology*. 4th ed. Philadelphia, PA: Lippincott Williams & Wilkins; 2001. p. 2675–705.
- [4] Koyano S, Inoue N, Oka A, Moriuchi H, Asano K, Ito Y, et al. Screening for congenital cytomegalovirus infection using newborn urine samples collected on filter paper: feasibility and outcomes from a multicentre study. *BMJ Open* 2011;1:e000118.
- [5] Fowler KB, Pass RF. Risk factors for congenital cytomegalovirus infection in the offspring of young women: exposure to young children and recent onset of sexual activity. *Pediatrics* 2006;118:e286–92.

- [6] Stratton KR, Durch JS, Lawrence RS. Vaccines for the 21st century. Washington, DC: National Academy Press; 2000.
- [7] Pass RF, Zhang C, Evans A, Simpson T, Andrews W, Huang ML, et al. Vaccine prevention of maternal cytomegalovirus infection. *N Engl J Med* 2009;360:1191–9.
- [8] Katano H, Sato Y, Tsutsui Y, Sata T, Maeda A, Nozawa N, et al. Pathogenesis of cytomegalovirus-associated labyrinthitis in a guinea pig model. *Microbes Infect* 2007;9:183–91.
- [9] Park AH, Gifford T, Schleiss MR, Dahlstrom L, Chase S, McGill L, et al. Development of cytomegalovirus-mediated sensorineural hearing loss in a Guinea pig model. *Arch Otolaryngol Head Neck Surg* 2010;136:48–53.
- [10] Woolf NK, Koehn FJ, Harris JP, Richman DD. Congenital cytomegalovirus labyrinthitis and sensorineural hearing loss in guinea pigs. *J Infect Dis* 1989;160:929–37.
- [11] Griffith BP, Lucia HL, Hsiung GD. Brain and visceral involvement during congenital cytomegalovirus infection of guinea pigs. *Pediatr Res* 1982;16:455–9.
- [12] Chatterjee A, Harrison CJ, Britt WJ, Bewtra C. Modification of maternal and congenital cytomegalovirus infection by anti-glycoprotein b antibody transfer in guinea pigs. *J Infect Dis* 2001;183:1547–53.
- [13] Schleiss MR, Bourne N, Stroup G, Bravo FJ, Jensen NJ, Bernstein DI. Protection against congenital cytomegalovirus infection and disease in guinea pigs, conferred by a purified recombinant glycoprotein B vaccine. *J Infect Dis* 2004;189:1374–81.
- [14] Schleiss MR, Bourne N, Bernstein DI. Preconception vaccination with a glycoprotein B (gB) DNA vaccine protects against cytomegalovirus (CMV) transmission in the guinea pig model of congenital CMV infection. *J Infect Dis* 2003;188:1868–74.
- [15] Griffith BP, McCormick SR, Fong CK, Lavalley JT, Lucia HL, Goff E. The placenta as a site of cytomegalovirus infection in guinea pigs. *J Virol* 1985;55:402–9.
- [16] Nozawa N, Yamamoto Y, Fukui Y, Katano H, Tsutsui Y, Sato Y, et al. Identification of a 1.6 kb genome locus of guinea pig cytomegalovirus required for efficient viral growth in animals but not in cell culture. *Virology* 2008;379:45–54.
- [17] Kanai K, Yamada S, Yamamoto Y, Fukui Y, Kurane I, Inoue N. Re-evaluation of the genome sequence of guinea pig cytomegalovirus. *J Gen Virol* 2011;92:1005–20.
- [18] Kanegae Y, Makimura M, Saito I. A simple and efficient method for purification of infectious recombinant adenovirus. *Jpn J Med Sci Biol* 1994;47:157–66.
- [19] Yamada S, Nozawa N, Katano H, Fukui Y, Tsuda M, Tsutsui Y, et al. Characterization of the guinea pig cytomegalovirus genome locus that encodes homologs of human cytomegalovirus major immediate-early genes, UL128, and UL130. *Virology* 2009;391:99–106.
- [20] Bourne N, Schleiss MR, Bravo FJ, Bernstein DI. Preconception immunization with a cytomegalovirus (CMV) glycoprotein vaccine improves pregnancy outcome in a guinea pig model of congenital CMV infection. *J Infect Dis* 2001;183:59–64.
- [21] McDonagh S, Maidji E, Chang HT, Pereira L. Patterns of human cytomegalovirus infection in term placentas: a preliminary analysis. *J Clin Virol* 2006;35:210–5.
- [22] Cui X, Meza BP, Adler SP, McVoy MA. Cytomegalovirus vaccines fail to induce epithelial entry neutralizing antibodies comparable to natural infection. *Vaccine* 2008;26:5760–6.
- [23] Gerna G, Sarasini A, Patrone M, Percivalle E, Fiorina L, Campanini G, et al. Human cytomegalovirus serum neutralizing antibodies block virus infection of endothelial/epithelial cells, but not fibroblasts, early during primary infection. *J Gen Virol* 2008;89:853–65.
- [24] Maidji E, McDonagh S, Genbacev O, Tabata T, Pereira L. Maternal antibodies enhance or prevent cytomegalovirus infection in the placenta by neonatal Fc receptor-mediated transcytosis. *Am J Pathol* 2006;168:1210–26.
- [25] Scott GM, Chow SS, Craig ME, Pang CN, Hall B, Wilkins MR, et al. Cytomegalovirus infection during pregnancy with maternofetal transmission induces a proinflammatory cytokine bias in placenta and amniotic fluid. *J Infect Dis* 2012;205:1305–10.
- [26] Maidji E, Nigro G, Tabata T, McDonagh S, Nozawa N, Shiboski S, et al. Antibody treatment promotes compensation for human cytomegalovirus-induced pathogenesis and a hypoxia-like condition in placentas with congenital infection. *Am J Pathol* 2010;177:1298–310.
- [27] Kaufmann P, Davidoff M. The guinea-pig placenta. *Adv Anat Embryol Cell Biol* 1977;53:5–91.

ORIGINAL RESEARCH COMMUNICATION

---

# Nitrosative Stress Induces Peroxiredoxin 1 Ubiquitination During Ischemic Insult *via* E6AP Activation in Endothelial Cells Both *In Vitro* and *In Vivo*

Rong-Rong Tao,<sup>1,\*</sup> Huan Wang,<sup>1,\*</sup> Ling-Juan Hong,<sup>1</sup> Ji-Yun Huang,<sup>1</sup> Ying-Mei Lu,<sup>2</sup> Mei-Hua Liao,<sup>1</sup> Wei-Feng Ye,<sup>1,3</sup> Nan-Nan Lu,<sup>1</sup> Dan-Yan Zhu,<sup>1</sup> Qian Huang,<sup>4</sup> Kohji Fukunaga,<sup>5</sup> Yi-Jia Lou,<sup>1</sup> Ikuo Shoji,<sup>6</sup> Christopher Stuart Wilcox,<sup>7</sup> En-Yin Lai,<sup>4,7</sup> and Feng Han<sup>1</sup>

## Abstract

**Aims:** Although there is accumulating evidence that increased formation of reactive nitrogen species in cerebral vasculature contributes to the progression of ischemic damage, but the underlying molecular mechanisms remain elusive. Peroxiredoxin 1 (Prx1) can initiate the antioxidant response by scavenging free radicals. Therefore, we tested the hypothesis that Prx1 regulates the susceptibility to nitrosative stress damage during cerebral ischemia *in vitro* and *in vivo*. **Results:** Proteomic analysis in endothelial cells revealed that Prx1 was upregulated after stress-related oxygen–glucose deprivation (OGD). Although peroxynitrite upregulated Prx1 rapidly, this was followed by its polyubiquitination within 6 h after OGD mediated by the E3 ubiquitin ligase E6-associated protein (E6AP). OGD colocalized E6AP with nitrotyrosine in endothelial cells. To assess translational relevance *in vivo*, mice were studied after middle cerebral artery occlusion (MCAO). This was accompanied by Prx1 ubiquitination and degradation by the activation of E6AP. Furthermore, brain delivery of a lentiviral vector encoding *Prx1* in mice inhibited blood–brain barrier leakage and neuronal damage significantly following MCAO. **Innovation and Conclusions:** Nitrosative stress during ischemic insult activates E6AP E3 ubiquitin ligase that ubiquitinates Prx1 and subsequently worsens cerebral damage. Thus, targeting the Prx1 antioxidant defense pathway may represent a novel treatment strategy for neurovascular protection in stroke. *Antioxid. Redox Signal.* 00, 000–000.

## Introduction

**B**RAIN MICROVASCULAR ENDOTHELIAL CELLS provide a barrier between the bloodstream and brain that is critical in brain development, maturation, and homeostasis (9, 37). The balance between endothelial cell survival and death is pivotal for brain remodeling and repair (41). Increased cell death of cerebrovascular endothelial cells exacerbates inflammatory, ischemic, and degenerative brain diseases (26). Before a new strategy can be developed to counter these

adverse effects of ischemia-induced endothelial dysfunction and neurovascular damage, it is necessary to define the factors responsible for ischemia-induced blood–brain barrier (BBB) damage.

Under conditions of intense oxidative stress, such as ischemia or hypoxia injury, increased generation of nitric oxide (NO) and superoxide ( $O_2^{\bullet-}$ ) results in the formation of peroxynitrite ( $ONOO^-$ ) (50). This is a short-lived highly reactive oxidant that attacks and inactivates many proteins. Specifically,  $ONOO^-$  irreversibly inactivates prostacyclin

---

<sup>1</sup>Institute of Pharmacology, Toxicology and Biochemical Pharmaceutics, Zhejiang University, Hangzhou, China.

<sup>2</sup>School of Medicine, Zhejiang University City College, Hangzhou, Zhejiang, China.

<sup>3</sup>The Children's Hospital, Zhejiang University School of Medicine, Hangzhou, China.

<sup>4</sup>Department of Physiology, Zhejiang University School of Medicine, Hangzhou, China.

<sup>5</sup>Department of Pharmacology, Graduate School of Pharmaceutical Sciences, Tohoku University, Sendai, Japan.

<sup>6</sup>Division of Microbiology, Center for Infectious Diseases, Kobe University Graduate School of Medicine, Kobe, Japan.

<sup>7</sup>Hypertension, Kidney, and Vascular Research Center, Georgetown University Medical Center, Washington, District of Columbia.

\*Both authors contributed equally to this work.

### Innovation

Our study is the first demonstration that nitrosative stress initiates the ubiquitination of peroxiredoxin 1 (Prx1) and subsequent disturbance of redox homeostasis in endothelial cells during ischemia-like injury. Our findings further identified E6-associated protein (E6AP) E3 ligase that ubiquitinated Prx1. Thus, repression of peroxynitrite (ONOO<sup>-</sup>) formation or *E6AP* knockdown dampened the ischemia-induced disturbance of Prx1 defense signaling. Since an active Prx1 was required for optimal neurovascular cell survival, targeting the Prx1 antioxidant defense pathway may represent a novel treatment strategy for neurovascular protection after stroke.

synthase and oxidizes tetrahydrobiopterin to dihydrobiopterin, thereby uncoupling endothelial NO synthase and directing it to generate O<sub>2</sub><sup>•-</sup> in place of NO. Indeed, endothelial cells are the primary targets of nitrosative stress in cardiovascular disease, stroke, and neurodegenerative disorders (18, 48). Although nitrosative damage to lipids, proteins, and DNA has been implicated in neurovascular damage following cerebral ischemia, the downstream signaling mechanisms remain elusive (13, 16, 17, 29).

Peroxiredoxins (Prxs) are thiol-specific antioxidant enzymes that maintain redox balance under both normal conditions and oxidative stress (6, 7, 10, 28). Although Prx1 is the most abundant and widely distributed member of the mammalian Prxs (23, 24) and is a recognized peroxide-detoxifying enzyme, its pathophysiological role during brain disease remains unclear (38, 44). Cultured *Prx1*-deficient fibroblasts have decreased proliferation and increased sensitivity to oxidative DNA damage. *Prx1*-deficient mice developed hemolytic anemia caused by increased erythrocytic reactive oxygen species (ROS) (34). Furthermore, mutant Huntington (*mHtt*) gene expression decreased Prx1 levels and increased its sulfenylation (35).

We tested the hypothesis that Prx1 in endothelial cells in culture and in the brain *in vivo* is a pivotal antioxidant pathway but can be damaged by nitrosative stress during hypoxia or ischemia, thereby exacerbating injury. We report that oxygen/glucose-deprived endothelial cells ubiquitinate Prx1 by nitrosative activation of E3 ubiquitin ligase (E6-associated protein [E6AP]). The outcome is that Prx1 is targeted for degradation leading to cellular redox imbalance and loss of the integrity of the endothelial BBB in mice following ischemia. Repression of ONOO<sup>-</sup> formation or *E6AP* knockdown dampened these disturbances of Prx1 defense signaling in endothelial cells. The initial study was made in human umbilical vascular endothelial cells, and key observations were confirmed and extended in human brain microvascular endothelial cells (HBMECs). Thus, our results indicate that Prx1 is a pivotal molecule for the protection of endothelial cells and microvessels from ischemia-induced neurovascular damage both *in vitro* and *in vivo*.

## Results

### Identification of differentially expressed proteins after oxygen–glucose deprivation in endothelial cells

Two-dimensional gel electrophoresis was performed in EA.hy926 endothelial cells to identify proteins that were

differentially expressed between control and oxygen–glucose deprivation (OGD)-treated endothelial cells. Figure 1A shows a silver-stained two-dimensional gel electrophoresis reference map of the OGD-treated endothelial cultures (Fig. 1A, *n* = 3, lower) in comparison to the control profile (Fig. 1A, *n* = 3, upper). The spots that showed a twofold or greater difference between treatments were further characterized by trypsin digestion and matrix-assisted laser desorption/ionization (MALDI) time-of-flight (TOF) mass spectrometry. Twenty-two different proteins from 36 spots were identified with high confidence (CI % ranging from 97.5% to 100%) (Supplementary Table S1; Supplementary Data are available online at [www.liebertpub.com/ars](http://www.liebertpub.com/ars)). The identified proteins were classified into functional groups (Supplementary Fig. S1). We selected Prx1 for further study since it was implicated in oxidation–reduction balance and abundantly increased 2.5-fold after OGD treatment (Supplementary Fig. S2A).

### Temporal changes of Prx1 protein levels in endothelial cells after OGD

Immunoblotting studies demonstrated a time-dependent increase in Prx1 over 1–6 h followed by a decline after 12 h (Fig. 1B, C). There was a similar pattern of protein levels of heat shock protein 27 (HSP27) (Fig. 1B, C). Molecular chaperones such as HSP27 can defend against protein misfolding after sublethal stressful stimuli (4). Immunocytochemical experiments demonstrated intracellular localization of Prx1 (Fig. 1D), which increased 6 h after OGD treatment in the cytosol of endothelial cells (Fig. 1D, E).

### Characterization of OGD-induced Prx1 ubiquitination in endothelial cells

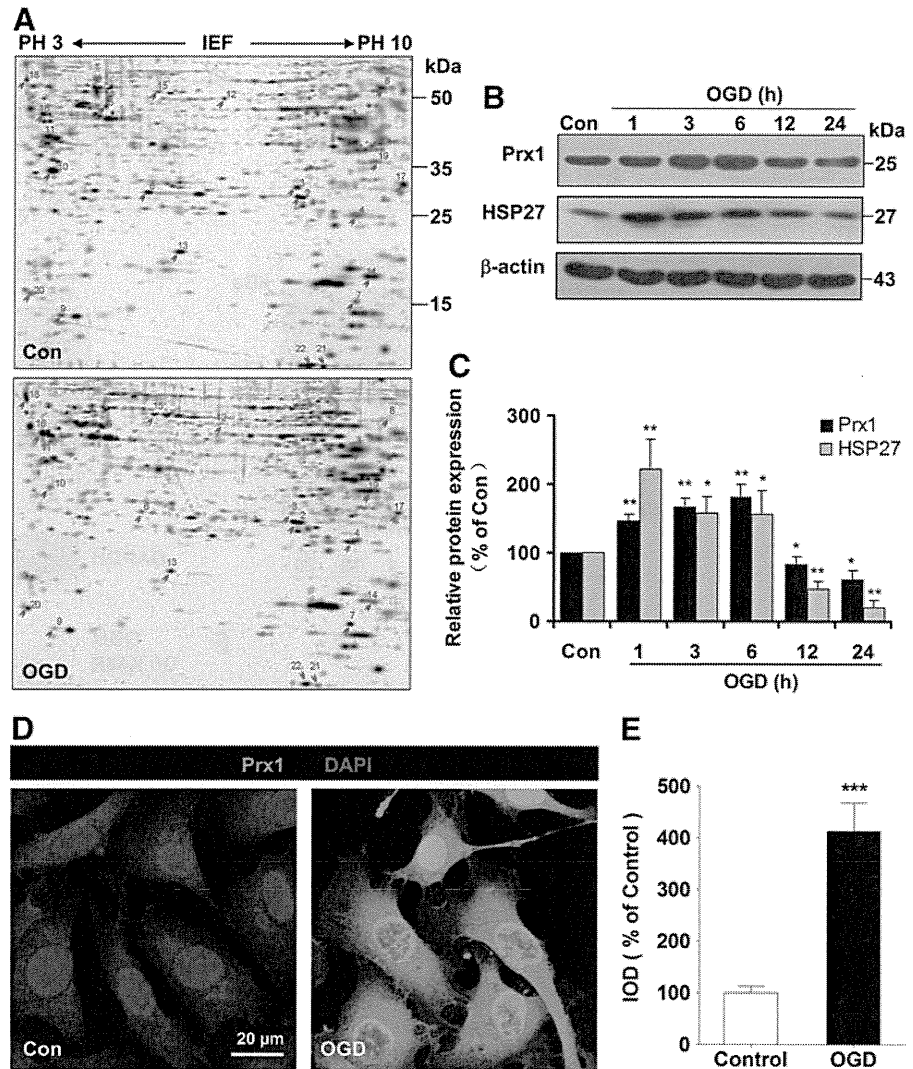
Unexpectedly, our western blot data demonstrated a continual increase in the density of a broad, high-molecular-weight (>118 kDa) band for Prx1 starting 6 h after OGD treatment (Fig. 2A). A similar increase in a high-molecular-weight band (>118 kDa) was detected following OGD treatment after probing with an anti-ubiquitin antibody (Fig. 2B). The OGD-induced ubiquitination of Prx1 was confirmed and extended in HBMECs (Fig. 3A, B) and mouse cerebral microvascular endothelial cells (bEnd.3) (Supplementary Fig. S2B).

Inhibition of proteosomal uptake with MG132 or lactacystin also increased the high-molecular-weight isoforms of Prx1 (Fig. 2C and Supplementary Fig. S3). Probing with an anti-Prx1 antibody in ubiquitin immunocomplexes from OGD-treated endothelial cells revealed a predominant band larger than 118 kDa (Fig. 2D and Fig. 3C). OGD-induced ubiquitination of Prx1 was confirmed by the immunoprecipitation of Prx1 followed by immunoblotting with an anti-ubiquitin antibody (Fig. 2E and Fig. 3D). Consistently, western blot analysis of cell extracts from OGD-treated cells demonstrated that high-molecular-weight conjugates of Prx1 were significantly reduced in *ubiquitin-K48R*-transfected endothelial cells (Fig. 2F and Fig. 3E, F).

### The role of Prx1 during proapoptotic cascades after OGD treatment

Proapoptotic proteins were identified by immunoblotting of EA.hy926 cells transfected with either an empty vector or

**FIG. 1. The proteomic identification of differentially expressed proteins after OGD in endothelial cells.** (A) Representative silver-stained two-dimensional gel of control and OGD-treated EA.hy926 endothelial cells. Whole proteins (450  $\mu\text{g}$ ) were separated on a non-linear pH gradient (3–10) followed by 12% SDS-PAGE. (B) Time course of Prx1 and HSP27 protein levels in cell lysates of endothelial cells following OGD. Quantifications of the temporal changes of Prx1 and HSP27 protein levels are shown in (C). Immunoblots are representative of three independent experiments.  $*p < 0.05$ ;  $**p < 0.01$  versus control. Immunoblotting with an anti- $\beta$ -actin antibody showed equal amounts of loaded protein in each lane. (D) Changes in the immunostaining of Prx1 (green) 6 h after OGD. Subcellular localization of Prx1 was determined by laser confocal microscopy. Data are representative of three independent experiments. Scale bar = 20  $\mu\text{m}$ . (E) Quantification of Prx1 immunofluorescence expressed as IOD as described in the Materials and Methods section.  $***p < 0.001$  versus control. IOD, integrated optical density; HSP27, heat shock protein 27; OGD, oxygen–glucose deprivation; Prx1, peroxiredoxin 1; SDS-PAGE, sodium dodecyl sulfate–polyacrylamide gel electrophoresis. To see this illustration in color, the reader is referred to the web version of this article at [www.liebertpub.com/ars](http://www.liebertpub.com/ars)



a *Prx1* expression vector following OGD insult (Fig. 4). Calnexin is a type I integral endoplasmic reticulum (ER) membrane chaperone involved in folding newly synthesized (glycol) proteins (8). Overexpression of Prx1 significantly inhibited calnexin, PERK, and Ire-1 $\alpha$  degradation (Fig. 4A, B) and also inhibited caspase-3 and poly ADP-ribose polymerase (PARP) cleavage (Fig. 4C, D). Exposure of vector-transfected cells to OGD for 6 h decreased the phosphorylation of anti-apoptotic proteins, such as phospho-ERK (Thr202/Tyr204) and phospho-FKHR (Ser256) (forkhead transcription factor Foxo1), and also decreased the protein levels of heme oxygenase-1 (HO-1) but increased the phosphorylation of c-Jun N-terminal kinase (JNK) and P38 (Fig. 4E, F). By contrast, overexpression of *Prx1* after OGD injury resulted in significant upregulation of anti-apoptotic proteins in endothelial cells (Fig. 4E, F). Exposure of vector-transfected cells to OGD for 6 h elevated terminal deoxynucleotidyl transferase dUTP nick end labeling (TUNEL)-positive staining (Fig. 4G, H), whereas overexpression of Prx1 effectively decreased TUNEL staining (Fig. 4G, H). The apoptosis of endothelial cells was determined using flow cytometry with Annexin V-FITC/propidium iodide (PI). In contrast to control cells (2.20%), we found that OGD treatment induced

elevation in the fraction of Annexin V/PI-positive cells (49.92%). Moreover, *Prx1* small interfering RNA (siRNA) transduction further exaggerated OGD-induced cell death (Fig. 4I). The present data demonstrate that Prx1 elicits an anti-apoptotic effect after OGD injury in endothelial cells, coinciding with its antioxidant function in the endothelium (31).

#### E6AP activation contributes to Prx1 stress response after OGD

Since Prx1 has been identified as a novel E6AP-binding protein (33), the present study further elaborates the role of E6AP in ubiquitination of Prx1 during OGD. Representative blots are presented in Figure 5A and show that E6AP was activated following OGD exposure over 1–24 h (Fig. 5A). Similar change of E6AP was confirmed in HBMEC (Supplementary Fig. S4A, B) and bEnd.3 endothelial cells after OGD (Supplementary Fig. S2B). Immunocytochemical analysis of the endothelial cells revealed OGD-induced strong immunoreactivity for E6AP (red fluorescence) that was undetectable in control cells (Fig. 5B–D and Supplementary Fig. S4C, D), which suggests that OGD-induced ubiquitination of Prx1 is associated with E6AP activation.

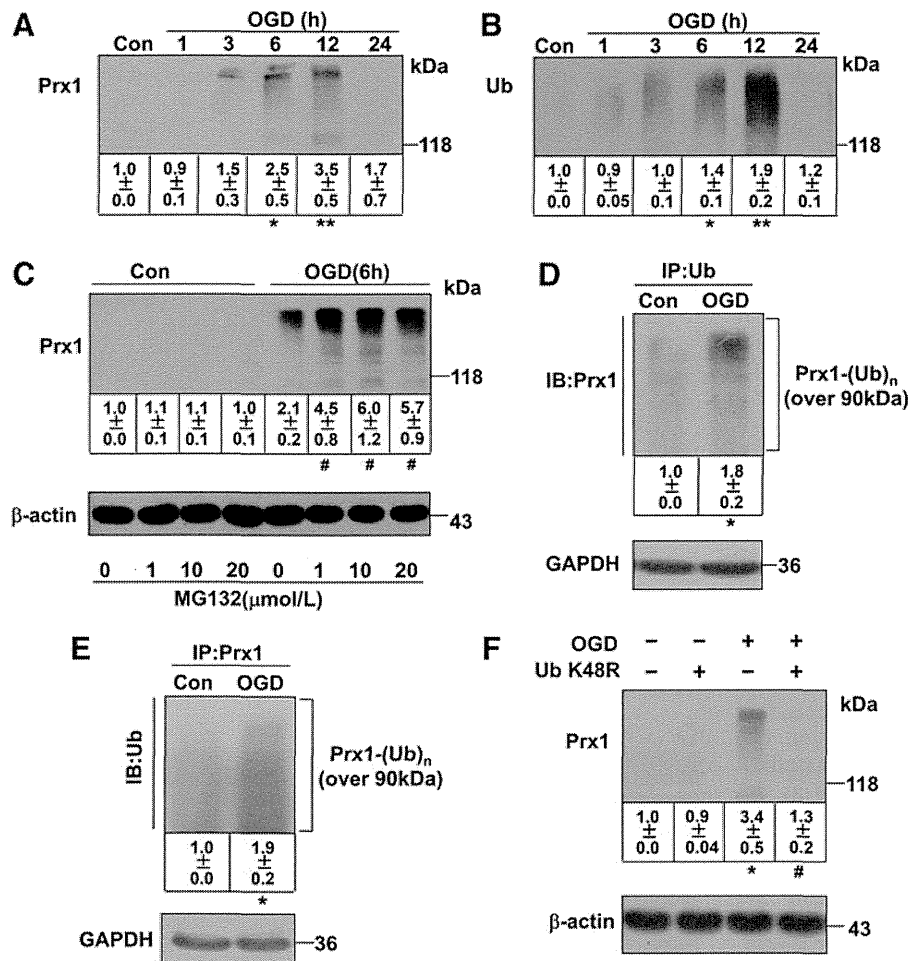


**FIG. 2. OGD induces ubiquitination of Prx1 in EA.hy926 endothelial cells.** (A) Temporal changes in the high-molecular-weight Prx1 isoform were observed in OGD-treated endothelial cells. The accumulated polyubiquitinated proteins were detected by western blot analysis with anti-Prx1 antibody. (B) Protein ubiquitination status after OGD treatment in endothelial cells. The accumulated multiubiquitinated proteins were detected by western blot analysis with an anti-ubiquitin antibody. (C) The changes in polyubiquitinated Prx1 were detected following OGD treatment of endothelial cells with or without proteasome inhibitors. The endothelial cells were treated with 1, 10, or 20  $\mu$ M MG132 or DMSO 30 min before OGD. The cells were then washed, harvested after 6 h OGD, and analyzed for polyubiquitinated Prx1 levels. (D) The OGD-induced ubiquitination of Prx1 was detected by the immunoprecipitation of ubiquitin followed by immunoblotting with an anti-Prx1 antibody. (E) Immunoprecipitation of Prx1 from cell lysates of OGD-treated endothelial cells followed by blotting with an anti-ubiquitin antibody. (F) The ubiquitin K48R mutant decreased OGD-induced Prx1 ubiquitination in endothelial cells. Endothelial cells were cultured and transfected with plasmid DNA encoding the *ubiquitin-K48R* mutant or an empty plasmid, followed by OGD and immunoblotting analysis. Immunoblots are representative of three independent experiments. Data are expressed as the percentage of values of control (mean  $\pm$  SEM). \* $p < 0.05$ ; \*\* $p < 0.01$  versus control; # $p < 0.05$  versus OGD.

E6AP and the active-site cysteine-to-alanine-inactivated mutant E6AP were expressed in mammalian *p3869HA-E6AP C-A* cells (22, 46). Here, after 48 h of transfection, siRNA knockdown of *E6AP* (Fig. 5E, F) or transfection with the *E6AP C-A* mutant (Fig. 5G, H) both significantly blunted the ubiquitination of Prx1 in OGD-treated endothelial cells.

#### Nitrosative stress associated with the Prx1 defensive response after OGD

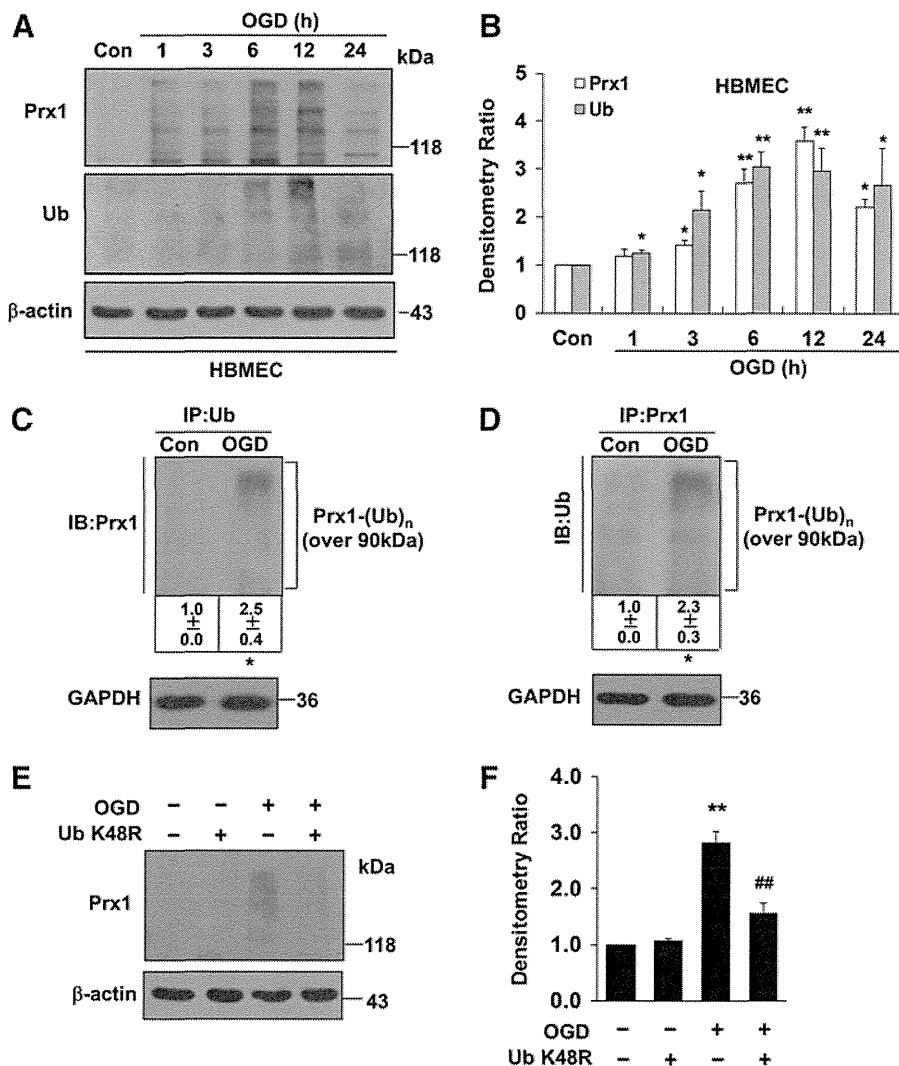
The ONOO<sup>-</sup> donor 3-morpholinopyridone (SIN-1) induced early dose-dependent elevation of Prx1 (Supple-

mentary Fig. S5A, B) and Prx1 ubiquitination (Fig. 6A, B) in endothelial cells as detected by immunoblot, accompanied by increased Prx1 immunostaining (Fig. 6C) and activation of E6AP (Fig. 6D). Whereas increased nitrotyrosine immunostaining and E6AP immunoreactivity were observed in OGD-treated cells (Fig. 6E, F), inhibition of ONOO<sup>-</sup> with uric acid markedly reduced both nitrotyrosine and E6AP immunostaining after OGD exposure (Fig. 6E). This was confirmed by western blot (Fig. 6G, H). A similar result was observed in endothelial cells treated with ONOO<sup>-</sup> decomposition catalysts (FeTPPS, 1  $\mu$ M) (Supplementary Fig. S6A, B). E6AP immunoprecipitates from the cell lysates were probed with anti-nitrotyrosine antibody (Fig. 6I). The results



**FIG. 3. The ubiquitination of Prx1 in OGD-treated HBMEC.**

(A) The time-dependent change of OGD-induced Prx1 and ubiquitin expression in HBMECs was detected by western blot. (B) Densitometry of the western blots for (A) was normalized by the level of  $\beta$ -actin as an internal control. (C) OGD-treated HBMEC endothelial cells were lysed and subjected to immunoprecipitation with antibodies to ubiquitin. The resultant precipitates were then subjected to immunoblot analysis with antibodies to Prx1. (D) Immunoprecipitation of Prx1 from lysed HBMEC with or without OGD treatment were collected for immunoblot analysis with ubiquitin antibody. (E) The *ubiquitin-K48R* mutant transfection attenuates Prx1 ubiquitination in OGD-treated endothelial cells. HBMEC were cultured and transfected with plasmid DNA encoding the *ubiquitin-K48R* mutant or an empty plasmid. (F) Densitometry of the western blots for (E) was normalized by the level of  $\beta$ -actin as an internal control. Immunoblots are representative of three independent experiments. Data are expressed as the percentage of values of control (mean  $\pm$  SEM). \* $p < 0.05$ ; \*\* $p < 0.01$  versus control; ### $p < 0.01$  versus OGD. HBMEC, human brain microvascular endothelial cell.



demonstrated that the E6AP/nitrotyrosine interaction in OGD-treated endothelial cells was significantly increased. Consistently, OGD-induced tyrosine nitration of E6AP was further confirmed by the immunoprecipitation of nitrotyrosine followed by immunoblotting with an anti-E6AP antibody (Fig. 6J). In addition, Prx1 immunoprecipitates from the lysates were probed with anti-nitrotyrosine antibody demonstrating that OGD did not induce Prx1 protein co-immunoprecipitate with nitrotyrosine (Supplementary Fig. S7). Melatonin blunted the ubiquitination of Prx1 in OGD-treated cells (Supplementary Fig. S8), suggesting that nitrosative stress induced Prx1 ubiquitination during OGD.

#### *E6AP activation contributes to Prx1 stress response in brain microvessels after transient middle cerebral artery occlusion in mice*

Since there are limited *in vivo* data on the degradation of Prx1 by ubiquitin ligases in ischemic brain, we used a mouse transient middle cerebral artery occlusion (tMCAO) model for further study. The immunoreactivity for E6AP was observed predominantly in the ipsilateral brain microvessel endothelium 6 h after tMCAO (Fig. 7A-e), accompanied by increased Prx1 immunoreactivity (Fig. 7A-d). A representa-

tive Z-stack image is shown in Figure 7B. However, after 24 h, Prx1 was downregulated where E6AP remained upregulated in the brain microvessel endothelium (Fig. 7A, g-i). Ubiquitination of Prx1 was elevated significantly in the brain microvessels 6 h after MCAO (Fig. 7C, D), whereas Prx1 staining was observed in microvessels of sham-operated animals where ubiquitin staining was absent. To further determine E6AP as a key modulator in nitrosative stress-mediated cerebrovascular damage *in vivo*, we stereotactically delivered a lentivirus carrying mouse *shE6AP* into the ventricle in mice 2 weeks before MCAO, followed by ischemia and 24 h reperfusion. Western blot analysis showed that lentivirus-mediated cerebral *E6AP* knockdown reduced cerebrovascular damage, which was demonstrated by preventing ischemia-induced dephosphorylation of prosurvival kinases and tight junction proteins breakdown (Fig. 7E-G).

#### *Lentiviral-Prx1 brain transduction protects against neurovascular damage in tMCAO mice*

Two weeks after the cerebroventricular injection of a lentiviral-GFP vector encoding mouse *Prx1* (LV-*Prx1*), there was efficient and sustained GFP fluorescence in the brain ventricles (Fig. 8A), cortex (Fig. 8B), hippocampus, and

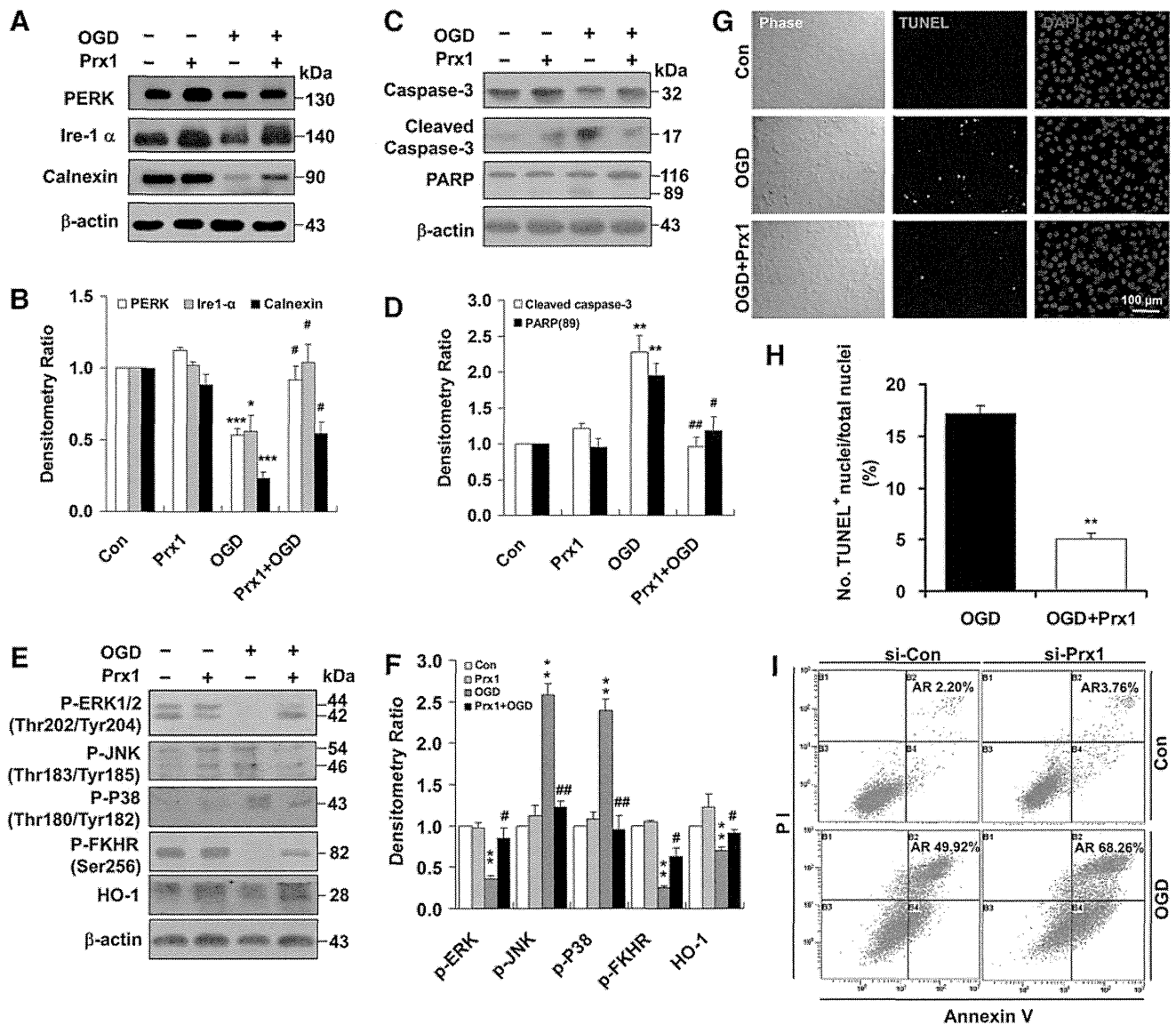


**FIG. 4. Role of Prx1 in the OGD-induced apoptotic cascade in endothelial cells.** (A) The effects of Prx1 on OGD-induced ER stress signaling were determined by immunoblotting. (B) Densitometry of western blots for PERK, Ire-1 $\alpha$ , and calnexin levels 6 h after OGD, with or without *Prx1* transfection. Data are expressed as densitometry ratio of control (mean  $\pm$  SEM). \* $p$  < 0.05; \*\*\* $p$  < 0.001 versus control; # $p$  < 0.05 versus OGD. (C) The effects of Prx1 overexpression on OGD-induced caspase-3 and PARP levels were evaluated by immunoblotting. EA.hy926 cells were cultured and transfected with plasmid DNA encoding *Prx1* or an empty plasmid using Attractene. (D) The quantification data for blots are shown in (C). Data are expressed as densitometry ratio of control (mean  $\pm$  SEM). \*\* $p$  < 0.01 versus control; # $p$  < 0.05; ## $p$  < 0.01 versus OGD. (E) The effects of Prx1 overexpression on OGD-induced protein levels were evaluated by immunoblotting. Cells were transfected with *Prx1* plasmid followed by 6 h of OGD or control stimulation. Cell lysates were prepared and resolved by SDS-PAGE. The proteins were immunoblotted with antibodies against phospho-ERK, phospho-JNK, phospho-P38, phospho-FKHR (Ser256), and HO-1. (F) Quantitative analysis of protein levels for (E) was performed by densitometry. Data are expressed as densitometry ratio of control (mean  $\pm$  SEM). \*\* $p$  < 0.01 versus control; # $p$  < 0.05; ## $p$  < 0.01 versus OGD. (G) Changes in apoptosis 6 h after OGD were detected using the TUNEL assay. Double staining was performed for TUNEL (green) and DAPI (blue). The representative images show the increased percentage of TUNEL-positive apoptotic endothelial nuclei (green fluorescence) 6 h after OGD. Scale bar = 100  $\mu$ m. (H) Quantification of TUNEL-positive apoptotic endothelial cells with or without *Prx1* transfection. Apoptosis was dramatically reduced following the overexpression of the *Prx1* gene in endothelial cells after OGD. \*\* $p$  < 0.01 versus OGD group. (I) Representative flow cytometric dot plots of apoptotic cells after OGD with or without *Prx1* siRNA transfection. Cultured EA.hy926 cells were stimulated for 6 h with OGD with or without *Prx1* siRNA transfection. Cells were double-stained with Annexin-V and PI and analyzed by FACS. Immunoblots are representative of three independent experiments.  $\beta$ -Actin was used as the loading control. DAPI, 4',6-diamidino-2-phenylindole; ER, endoplasmic reticulum; HO-1, heme oxygenase-1; JNK, c-Jun N-terminal kinase; PARP, poly ADP-ribose polymerase; siRNA, small interfering RNA; TUNEL, terminal deoxynucleotidyl transferase dUTP nick end labeling; PI, propidium iodide. To see this illustration in color, the reader is referred to the web version of this article at [www.liebertpub.com/ars](http://www.liebertpub.com/ars)

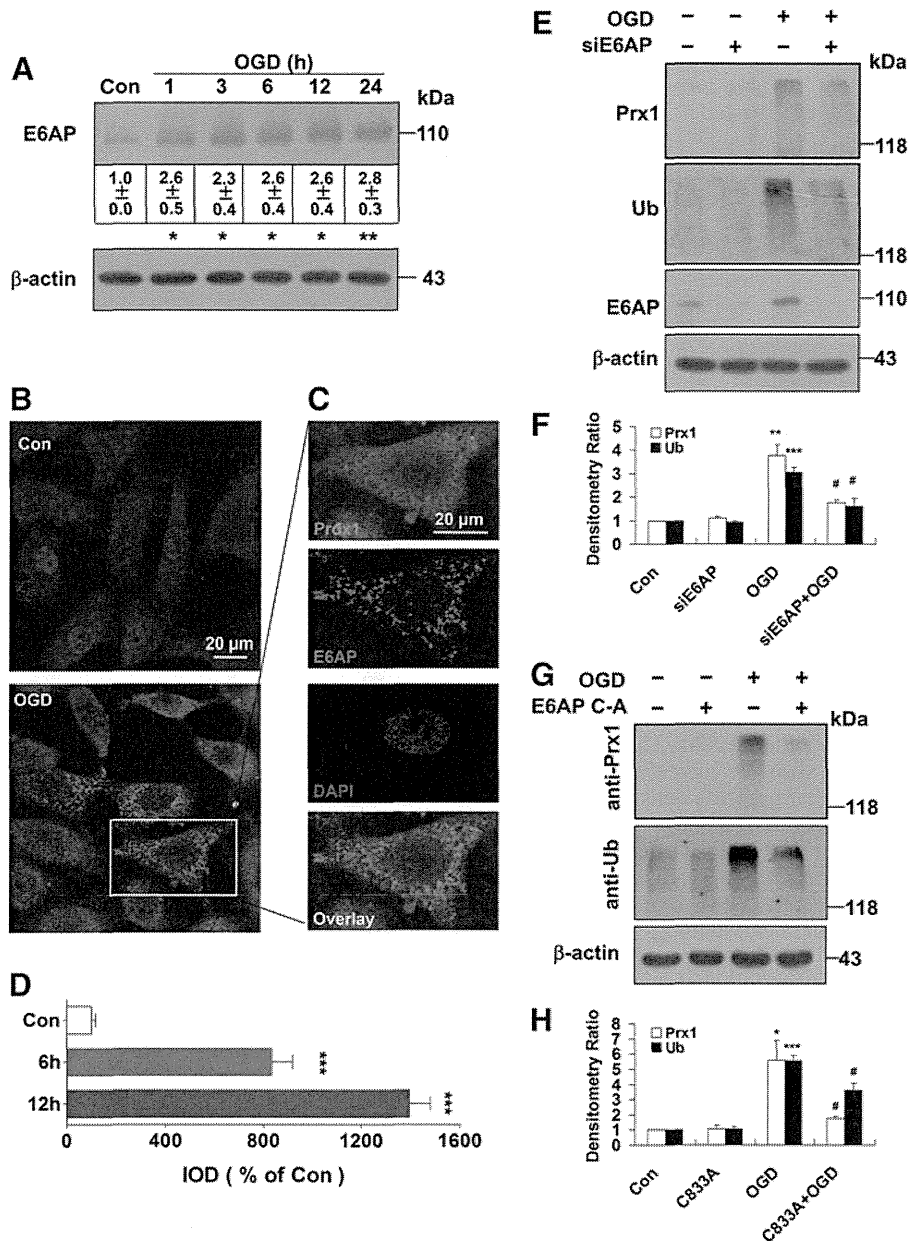


**FIG. 5. E6AP activation contributes to the Prx1 stress response after OGD.** (A) The representative image showing E6AP activation at the indicated time points after OGD treatment. Data are expressed as densitometry ratio of control (mean ± SEM). \* $p < 0.05$ ; \*\* $p < 0.01$  versus control. (B) Immunocytochemical analysis of E6AP expression after OGD treatment. Laser confocal microscopy demonstrated low to undetectable levels of E6AP in control cells. (C) Higher-magnification image of endothelial staining from the insets of (B). DAPI counterstaining indicates nuclear localization (blue). Scale bar = 20  $\mu\text{m}$ . (D) Quantification of Prx1 immunofluorescence expressed as integrated optical density (IOD). \*\*\* $p < 0.001$  versus control. (E) E6AP knockdown reduced the OGD-induced formation of multiubiquitinated proteins. Cells were submitted to E6AP knockdown and OGD or the control condition for 6 h. Cell lysates were prepared and resolved by SDS-PAGE. The proteins were immunoblotted with antibodies against Prx1, E6AP, and ubiquitin. (F) Quantitative analyses for (E) are shown in the bar graph as densitometry ratio of control (mean ± SEM). \*\* $p < 0.01$ ; \*\*\* $p < 0.001$  versus control; # $p < 0.05$  versus OGD. (G) The E6AP<sub>C-A</sub> mutant decreased OGD-induced Prx1 ubiquitination in endothelial cells. EA.hy926 cells were cultured and transfected with plasmid DNA encoding the E6AP<sub>C-A</sub> mutant or an empty plasmid using Attractene. (H) Quantitative analysis of protein levels for (G) was performed by densitometry. Data are expressed as densitometry ratio of control (mean ± SEM). \* $p < 0.05$ ; \*\*\* $p < 0.001$  versus control; # $p < 0.05$  versus OGD. Immunodetection of  $\beta$ -actin was used as a loading control. Immunoblots are representative of three independent experiments. E6AP, E6-associated protein. To see this illustration in color, the reader is referred to the web version of this article at [www.liebertpub.com/ars](http://www.liebertpub.com/ars)

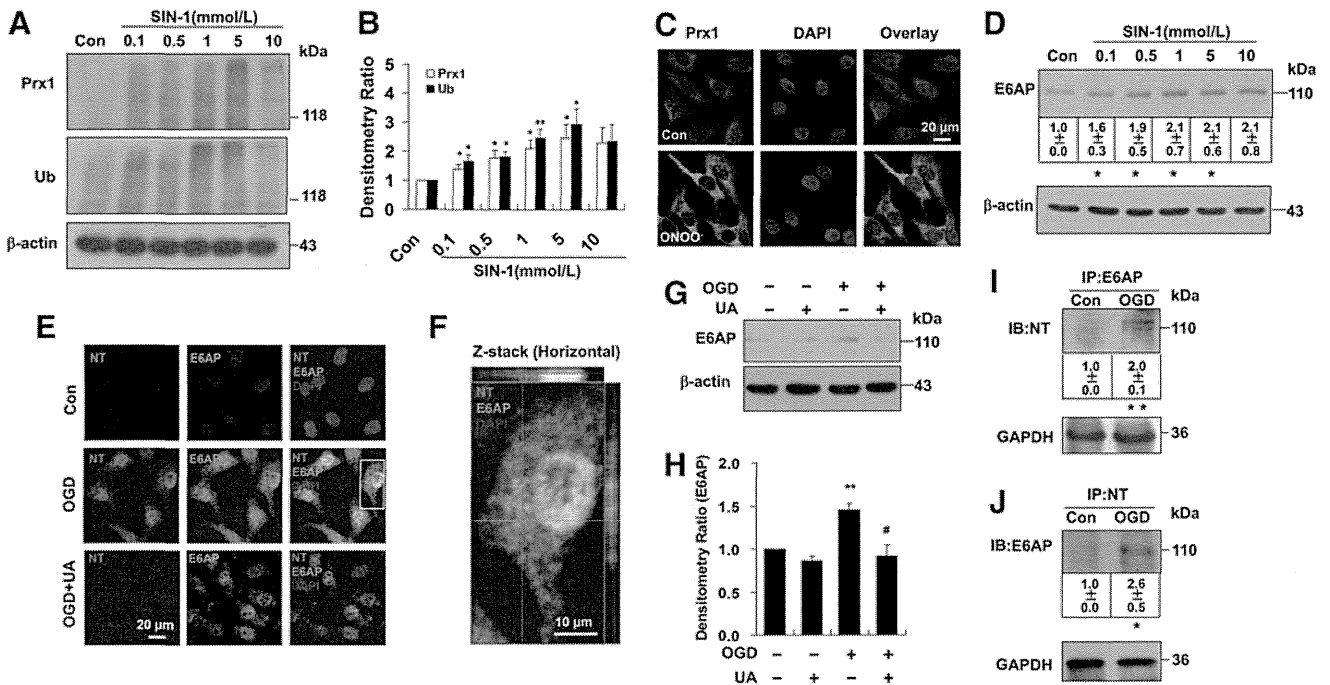


**FIG. 6. Nitrosative stress is associated with ubiquitination of Prx1 in endothelial cells.** (A) The ubiquitination of Prx1 after SIN-1 stimulation in endothelial cells. The blots were labeled with anti-Prx1 or anti-ubiquitin antibody and visualized with the ECL system. Molecular sizes are indicated on the right. (B) The SIN-1-induced changes in polyubiquitinated Prx1 were quantified and shown in the bar graph as densitometry ratio of control (mean  $\pm$  SEM). \* $p$  < 0.05; \*\* $p$  < 0.01 versus control. (C) Immunocytochemical analysis of Prx1 level after ONOO<sup>-</sup> treatment by laser confocal microscopy. DAPI counterstaining indicates nuclear localization (blue). (D) The effects of SIN-1 treatment on E6AP protein levels were examined in cell lysates of endothelial cells. EA.hy926 endothelial cells were cultured with or without SIN-1 treatment for 6 h at the indicated concentrations. Immunoblots are representative of three independent experiments (mean  $\pm$  SEM). \* $p$  < 0.05 versus control. (E) Fluorescence immunocytochemical staining of E6AP and nitrotyrosine 6 h after OGD in endothelial cells with or without 0.5 mM uric acid treatment. DAPI counterstaining indicates nuclear localization (blue). NT, nitrotyrosine; UA, uric acid. (F) Higher-magnification image of endothelial staining from the insets is shown in (E). (G) Effect of uric acid on E6AP expression in endothelial cells following OGD. Immunodetection of  $\beta$ -actin was used as a loading control. (H) Quantification of E6AP protein levels was performed using densitometric analysis of the immunoblots in (G). Immunoblots are representative of three independent experiments. Data are expressed as the percentage of values of control (mean  $\pm$  SEM). \*\* $p$  < 0.01 versus control; # $p$  < 0.05 versus OGD. (I) Immunoprecipitation of E6AP from cell lysates of OGD-treated endothelial cells followed by blotting with an anti-nitrotyrosine antibody. \*\* $p$  < 0.01 versus control. (J) The OGD-induced nitration of E6AP was detected by the immunoprecipitation of nitrotyrosine followed by immunoblotting with an anti-E6AP antibody. Immunoblots are representative of three independent experiments (mean  $\pm$  SEM). \* $p$  < 0.05 versus control. SIN-1, 3-morpholinosydnonimine. To see this illustration in color, the reader is referred to the web version of this article at [www.liebertpub.com/ars](http://www.liebertpub.com/ars)

striatum (Supplementary Figs. S9 and S10). Staining of brain sections from lentiviral-GFP-injected mice with a neuronal nuclear marker (NeuN) (Fig. 8B-d) and an endothelial marker CD31 (Fig. 8B-e, f) indicates that the vector successfully transduced cells in the brain. Although the lentiviral vectors might directly diffuse into the brain parenchyma, the present data indicate that lentiviral vectors in cerebral ventricular can diffuse along the neurovascular scaffold. Immunohistochemical analysis of ipsilateral sections revealed stronger GFP fluorescence in tMCAO mice that formed a continuous interendothelial staining pattern that colocalized with CD31 (Fig. 8C, D).

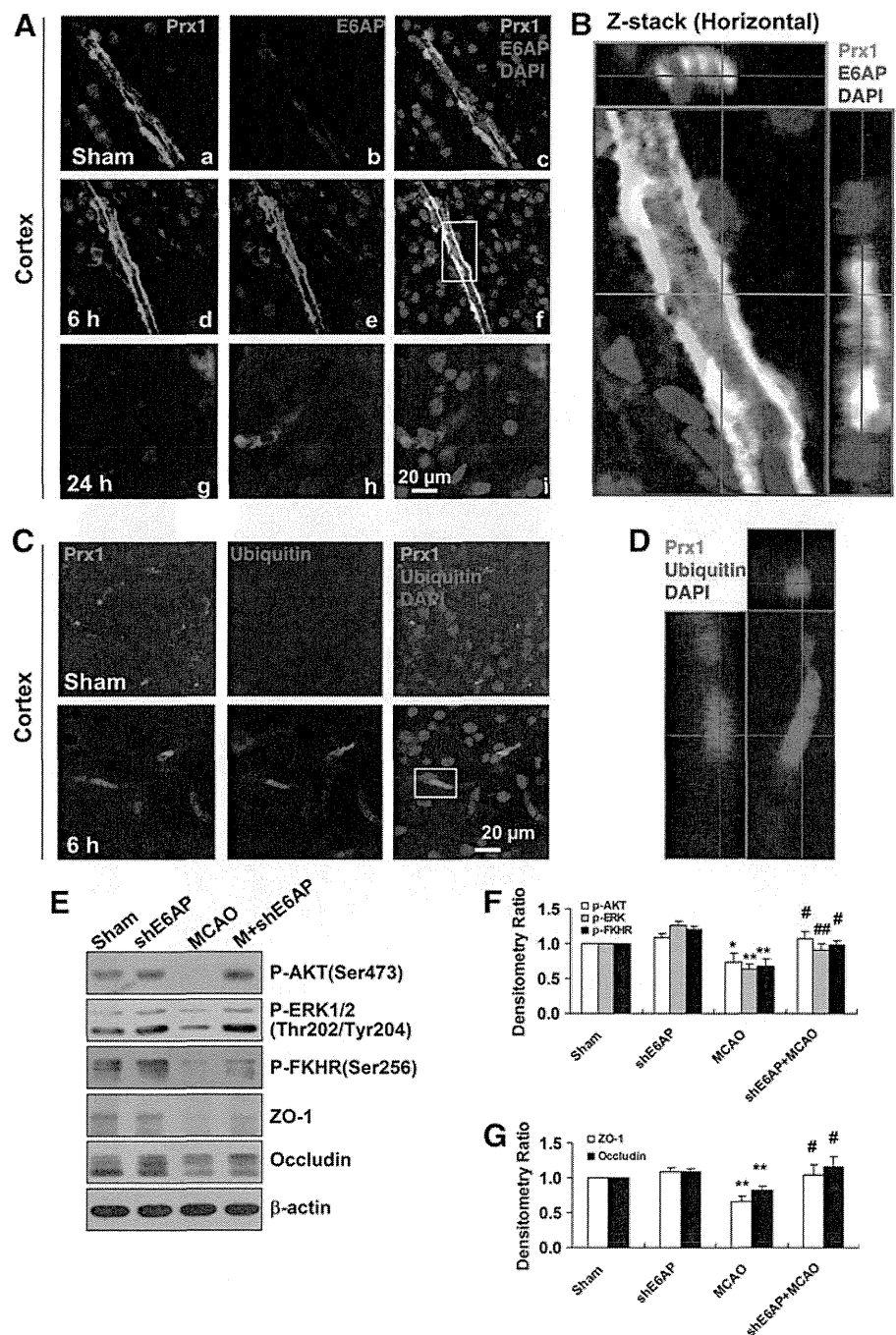
The protective effects of Prx1 against ischemia-induced neurological and functional deficit were evaluated by the rotarod test and neurological score measurements. The neurological scores were decreased significantly, and rotarod time was increased in LV-Prx1-treated mice 24 h after tMCAO (Fig. 9A) and the infarct area was reduced accordingly (Fig. 9B). The breakdown products of spectrin and

calcein were increased after tMCAO (Fig. 9C, D), coincident with BBB leakage (Fig. 9E, F). LV-Prx1 treatment blocked the degradation of tight junction proteins zonula occludens-1 (ZO-1) and claudin5 (Fig. 9C, D, and G) and significantly reduced BBB leakage (Fig. 9E, F). LV-Prx1 transduction reduced the O<sub>2</sub><sup>•-</sup> level assessed from dihydroethidium staining in the penumbra region of mice 24 h after tMCAO (Fig. 9H, I).

#### Schematic illustration of the mechanisms by which nitrosative stress induces Prx1 ubiquitination during ischemic insult in endothelial cells

We hypothesize that ischemia-induced nitrosative stress causes an early increase in Prx1 production during the adaptive phase, whereas excessive or prolonged ischemia activates E6AP E3 ubiquitin ligase, which targets Prx1 for ubiquitination and degradation during the late phase, thereby degrading the Prx1-related antioxidant defense pathway and

**FIG. 7. E6AP activation is associated with Prx1 ubiquitination in brain microvessels of cerebral ischemia mice.** (A) Double immunohistochemical staining for Prx1 and E6AP in the penumbra after tMCAO. Fluorescence staining for Prx1 (green) and E6AP (red) was performed in ipsilateral brain regions 6 and 24 h after brain ischemic injury in mice. (B) The orthogonal projections onto the  $x-z$  (upper) and  $y-z$  (right) planes are shown to confirm the colocalization of Prx1 and E6AP throughout the microvessels shown in (A). (C) Fluorescence immunohistochemical staining of Prx1 and ubiquitin in brain microvessels. Anti-ubiquitin (red) and Prx1 (green) staining was performed 6 h after tMCAO in mice. (D) Higher-magnification image of endothelial staining from the insets is shown in (C). Each image shown is representative of five independent mice. (E) The effect of E6AP knockdown on neurovascular damage after brain ischemia in mice. The lentivirus E6AP shRNA knockdown was used to silence E6AP mRNA. The protein extracts from penumbra brain region of mice were processed for western blotting to detect ZO-1, Occludin, and phosphorylated AKT, ERK, FKHR. (F, G) Quantitative analysis of protein levels in (E) was performed by densitometry. Densitometry values were normalized to the average of all sham values (mean  $\pm$  SEM,  $n=6$ ). \* $p < 0.05$ ; \*\* $p < 0.01$  versus sham mice; # $p < 0.05$ ; ### $p < 0.01$  versus vehicle-treated mice. Immunoblotting with an anti- $\beta$ -actin antibody demonstrated equal protein loading in each lane. tMCAO, transient middle cerebral artery occlusion; ZO-1, zonula occludens-1; shRNA, short hairpin RNA. To see this illustration in color, the reader is referred to the web version of this article at [www.liebertpub.com/ars](http://www.liebertpub.com/ars)



rendering the endothelial cells in the microvessels susceptible to ischemic damage (Fig. 10).

## Discussion

The present study demonstrates that in endothelial cells OGD treatment leads to oxidative and nitrosative stress that engage an early increase in Prx1 production and an antioxidant response. However, more prolonged or severe ischemia-mediated nitrosative stress ubiquitinates Prx1 by the activation of E6AP ligase, thereby degrading this antioxidant defense pathway. The translational studies in mice after MCAO demonstrated that neurovascular protection was coordinated by active Prx1.

Prx1 initiates the antioxidant response by scavenging free radicals formed in response to a diverse array of cellular stresses (40, 44). Upregulation of Prx1 may be secondary to the activation of NF-E2-related factor 2 (Nrf2) (24), as *Prx1* promoter has two antioxidant response elements that are putative binding sites for Nrf2. Indeed, we recently demonstrated that Nrf2 signaling coordinates the defense against ischemia/nitrosative stress in endothelial cells (49).

The ubiquitin-proteasome system is important for protein degradation in eukaryotic cells (19, 42). Unexpectedly, ubiquitin was not highly expressed in control endothelial cells, but high-molecular-weight Prx1-polyubiquitin ladders were observed after OGD or SIN-1 treatment. The aggregation of

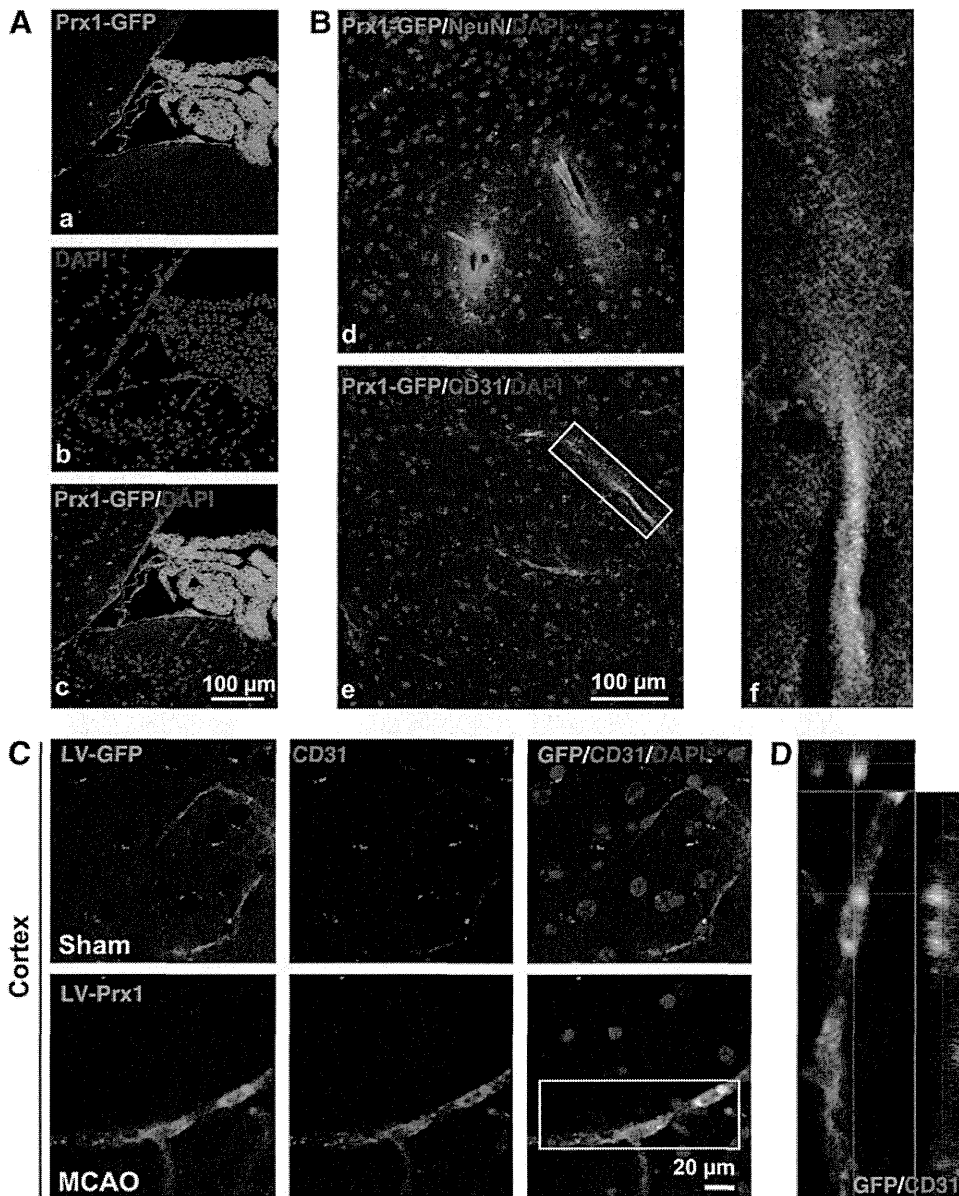


**FIG. 8.** The brain microvessels are the primary cell type transduced by the LV-GFP vector in the ipsilateral side of tMCAO mice. (A) The distribution of LV-GFP-Prx1 in the choroid plexus of the mouse brain 2 weeks after intracerebroventricular injection. Images demonstrate successful LV-GFP-Prx1 transduction in choroid plexus cells. (B) The immunohistochemical localization of NeuN-labeled cells (red) in (d) and CD31-marked cells (red) in (e) were examined in brain cortex of mice. The inset (f) showing magnified images from (B-e) demonstrates the localization of GFP-Prx1 in the microvessels of the brain. (C) Representative immunostaining demonstrates that CD31 (red) colocalized with GFP-Prx1 on the ipsilateral side of the brain cortex 24 h after MCAO. (D) Representative Z-stack images shown in (C). Each image shown is representative of five independently injected mice. NeuN, neuronal nuclear marker. To see this illustration in color, the reader is referred to the web version of this article at [www.liebertpub.com/ars](http://www.liebertpub.com/ars)

ubiquitinated Prx1 proteins in endothelial cells after OGD reflects an imbalance between the amount of toxic unfolded proteins and the capacity of the proteasomal system to eliminate them, which may culminate in ER stress. Consistent with our *in vitro* data, there was an increased ubiquitination of Prx1 in brain microvessels of mice following MCAO that was associated with endothelial/microvessel injury. The formation of ubiquitin-protein conjugates (ubi-proteins) may mediate ischemic cell death (19, 51). A time-dependent increase in E6AP after OGD induced Prx1 ubiquitination (33). The upregulation and colocalization of E6AP with Prx1 after OGD was blunted by inhibition of nitrosative stress with uric acid or FeTPPS.

Our results identify E6AP as the E3 ligase that targets Prx1 for degradation in the later phases of OGD. Accordingly, we tested the functional relevance of this pathway in protecting the BBB of mice during tMCAO. Brain ischemia increased E6AP expression in microvessels of the penumbra region.

Nitrosative stress from the reaction of NO generated by NO synthases in damaged brain cells and  $O_2^{\bullet-}$  generated during ischemia underlays the ischemic cerebral cell death (17, 48). We speculate from our endothelial cell model that ischemic nitrosative stress induced the overproduction of brain microvascular E6AP. Indeed, the computational predictor evaluated 7 potential tyrosine nitration sites of E6AP with high score (Supplementary Fig. S11). Additionally, S-nitrosylation has been shown to modify the function of many proteins (1, 32). Therefore, it will also be important to further characterize the protein S-nitrosylation of thiol and amine groups during ischemia in the future.

Our finding that inhibition of nitrosative stress and redirection of E6AP restored Prx1 signaling in endothelial cells defines a new vasoprotective mechanism against the damaging consequences of ischemia. This was exemplified by the demonstration that Prx1 overexpression in the intact brain blocked tMCAO-induced neurovascular damage, attenuated

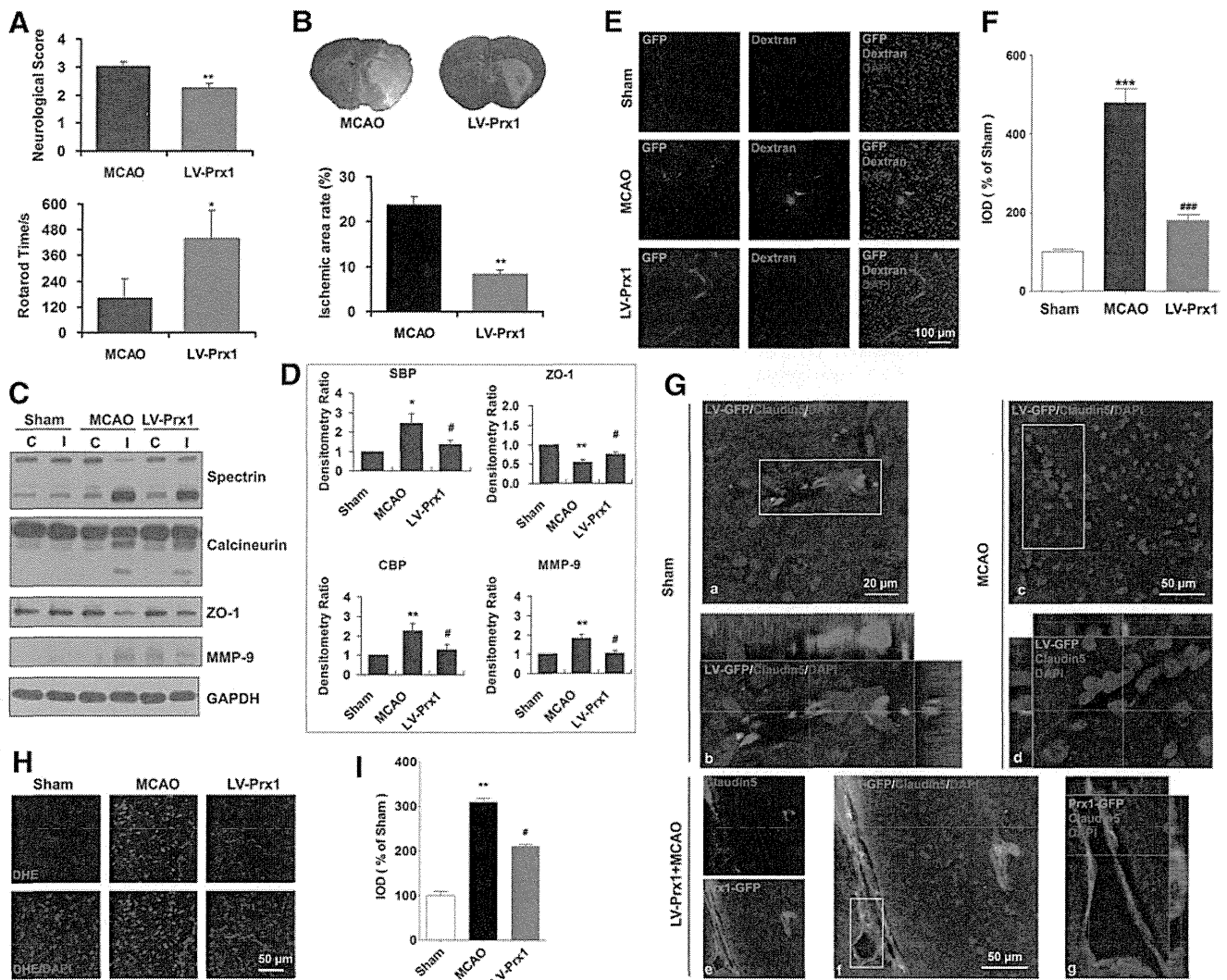


**FIG. 9. Lentiviral-mediated delivery of Prx1 protects against neurovascular protection in tMCAO mice.** (A) Lentiviral-mediated delivery of Prx1 improved neurological functional recovery after focal ischemia. The neurological scores (*upper*) and rotarod test (*lower*) were examined. The data are expressed as the percentage of the values observed in vehicle-treated animals (mean  $\pm$  SEM,  $n = 10$ ). \* $p < 0.05$ ; \*\* $p < 0.01$  versus vehicle-treated mice. (B) LV-Prx1 transduction reduced the infarct area of mice 24 h after tMCAO. The mice were subjected to 45 min of MCAO, and the infarct area was quantified 24 h later in cresyl violet-stained brain sections. The data are expressed as the percentage of the infarct area/total area of each brain section (mean  $\pm$  SEM,  $n = 10$ ). \*\* $p < 0.01$  versus vehicle-treated mice. (C) The effect of LV-Prx1 on neurovascular damage after brain ischemia. The proteins from penumbra brain region of mice were immunoblotted with antibodies against spectrin, calcineurin, ZO-1, and MMP-9, which are indicative antibodies for neurovascular damage. C, contralateral; I, ipsilateral. (D) The quantitative analyses are shown in the bar graph as the percentage of values of sham-operated animals (mean  $\pm$  SEM,  $n = 4$ ). \* $p < 0.05$ ; \*\* $p < 0.01$  versus sham mice; # $p < 0.05$  versus vehicle-treated mice. Immunoblotting with an anti- $\beta$ -actin antibody demonstrated equal protein loading in each lane. SBP, spectrin breakdown products; CBP, calcineurin breakdown products. (E) LV-Prx1 transduction attenuated BBB disruption 24 h after tMCAO. Mice were intravenously injected with Texas red-dextran in saline and perfused 120 min later. *Ex vivo* dextran labeling (red fluorescence) indicated extensive BBB permeability around disrupted brain microvessels in tMCAO mice. (F) Quantification of Texas red-dextran immunofluorescence expressed as integrated optical density (IOD). \*\*\* $p < 0.001$  versus sham; ### $p < 0.001$  versus vehicle-treated mice. (G) Effect of LV-Prx1 transduction on the degradation of claudin5. (a) Immunostaining with anti-claudin5 (red fluorescence) antibody showed brain ischemia-induced claudin5 degradation (c, d) in the microvessels 24 h after tMCAO. LV-Prx1 transduction reduced the degradation of claudin5 (e–g) in the microvessels 24 h after tMCAO. Higher-magnification images of microvessel staining (b, d, g) from the insets of (a, c, f), respectively. (H) The effect of Prx1 transduction on  $O_2^{\bullet-}$  levels, as determined by *in situ* dihydroethidium staining. LV-Prx1 transduction reduced the  $O_2^{\bullet-}$  level in the penumbra region compared to vehicle. Each image shown is representative of five independently injected mice. DHE, dihydroethidium. (I) The quantitative analyses of dihydroethidium immunofluorescence are shown in the bar graph. \*\* $p < 0.01$  versus sham; # $p < 0.05$  versus vehicle-treated mice. BBB, blood–brain barrier;  $O_2^{\bullet-}$ , superoxide. To see this illustration in color, the reader is referred to the web version of this article at [www.liebertpub.com/ars](http://www.liebertpub.com/ars)

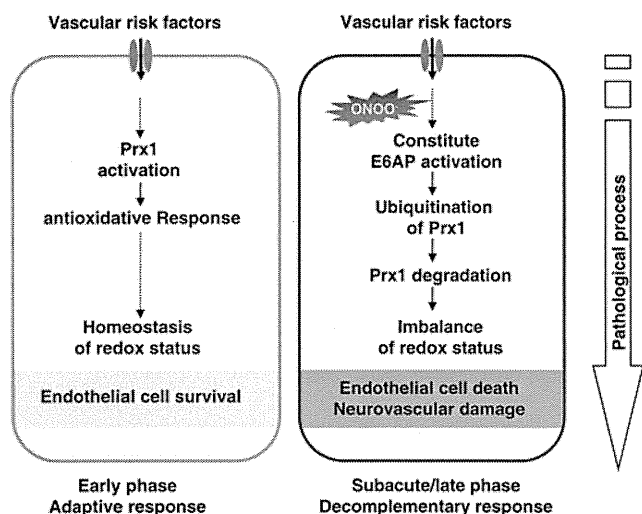


**FIG. 10. Schematic illustration of the mechanisms by which nitrosative stress induces Prx1 ubiquitination in endothelial cells during ischemic insult via E6AP activation.** To see this illustration in color, the reader is referred to the web version of this article at [www.liebertpub.com/ars](http://www.liebertpub.com/ars)

BBB damage, preserved the ZO-1, and prevented the activation of metalloproteinases (MMPs). This is similar to the reports that Prx1 was required also for neurovascular cell survival during exposure to pathogenic proteins associated with brain ischemia or with amyloid- $\beta$  expression in neurons (30). These results are consistent with the finding that *Prx1*-deficient mice suffer embryonic lethality because they lack essential antioxidant function (25, 34, 39). Although the neurovascular cells might be a critical issue during the earlier phase of brain ischemia, the functional coupling and collaborations among the capillaries, glia, and neurons of the brain should be taken into consideration (9, 37). For instance, recent studies highlight that pericyte loss causes BBB breakdown and neurodegeneration (2, 36). Therefore, how Prx1-mediated vascular protection contributed to the neuronal survival in the present study, however, is a topic for further investigation. Prx1 protein levels can prevent excessive ROS accumulation by interaction with thioredoxin to detoxify hydrogen peroxide ( $H_2O_2$ ),  $ONOO^-$ , and a range of organic hydroperoxides (34). We found further that LV transduction reduced  $O_2^{\bullet-}$  formation in the ipsilateral region of the ischemia brain, which might be a consequence of ERK and FKHR activation by Prx1. Indeed, Prxs participate in a very wide range of reactions, including neuronal differentiation, cell signaling, molecular chaperoning, and mitochondrial function, in both catalytic-dependent and catalytic-independent manners and can interact with JNK, c-Abl, and apoptosis signal-regulating kinase 1 (ASK1) in a redox-regulated manner (11, 14, 21, 23). Here, ipsilateral sections showed stronger GFP fluorescence in cerebral vessels of tMCAO mice, it might due to the changes of structural integrity in ischemic region, where dividing cell also largely accumulated (12, 20).

In summary, our studies identify an intracellular link between nitrosative stress and Prx1 signaling in endothelial cells following ischemia-like injury. Our description of an early ischemia-induced activation of beneficial Prx1 generation followed by subsequent inactivation represents a pre-

viously undescribed, nitrosative stress-dependent process mediated by E6AP-dependent Prx1 ubiquitination and subsequent endothelial barrier damage. Since Prx1 protected against oxidative stress in endothelial cells to reduce injury after ischemia, both *in vitro*- and *in vivo*-specific inducers of the Prx1 pathway, or mechanisms to prevent its degradation, may be targeted for therapeutic benefit in neurovascular disorders.

## Materials and Methods

### Reagents

Dulbecco's modified Eagle's medium (DMEM) and fetal bovine serum were purchased from Gibco. Alexa Fluor 488-conjugated anti-rabbit IgG and Alexa Fluor 594-conjugated anti-mouse IgG were obtained from Invitrogen. Uric acid was obtained from Wako. 5,10,15,20-Tetrakis-[4-sulfonatophenyl]-porphyrinato-iron[III] (FeTPPS; Calbiochem) was used as a specific  $ONOO^-$  decomposition catalyst. Unless otherwise stated, all reagents and chemicals were obtained from Sigma-Aldrich.

### OGD exposure and experimental treatments of cell cultures

EA.hy926 cells (16, 43), HBMECs, and mouse brain microvascular endothelial cells (bEnd.3) were used for western blot or immunocytochemistry in the present study. Briefly, in the oxygen and glucose deprivation phase, the culture medium was replaced and washed with glucose-free Hank's balanced salt solution, after which the cultures were placed in an airtight experimental hypoxia chamber (Billups-Rothenberg) containing a gas mixture comprising 95%  $N_2$  and 5%  $CO_2$ . To mimic an ischemia-like condition *in vitro*, cell cultures were exposed to OGD for 1, 3, 6, 12, and 24 h. Cells without OGD served as controls.

### Two-dimensional gel electrophoresis

Approximately 450  $\mu$ g of protein was resuspended in a rehydration solution [8 M Urea, 2% CHAPS, 20 mM DTT, 0.2% Biolyte (pH range 3–10), and 0.2% Bromphenol blue] and applied to 17-cm pH 3–10 nonlinear gradient immobilized strips for isoelectric focusing. Isoelectric focusing was performed using Protean IEF Cell (Bio-Rad), and the proteins in the IPG strips were subsequently placed on a 12% uniform sodium dodecyl sulfate (SDS)-polyacrylamide gel. The gels were silver stained and scanned with an Image Scanner in transmission mode, after which image analysis was conducted with two-dimensional PDquest (Bio-Rad). The two-dimensional gel electrophoresis was repeated three times using independently grown cultures.

### In-gel digestion and mass spectrometry analysis

The in-gel digestion of proteins for mass spectrometric characterization was performed as published previously (47). After the tryptic peptide mixture was dissolved with 0.5% trifluoroacetic acid, peptide mass analysis was performed using an AB4800 MALDI-TOF/TOF mass spectrometer (Applied Biosystems). The mass spectra were externally calibrated with a peptide standard from Applied Biosystems. Based on the National Center for Biotechnology Information



(NCBI) human databases, the mass spectra were analyzed with a 50 ppm mass tolerance by GPS Explorer version 2.0.1 and Mascot version 1.9.

#### Plasmid constructs and transfections

The EA.hy926 or HBMEC endothelial cells were cultured in six-well plates in the growth medium and transfected with plasmid DNA encoding *Prx1*, *siPrx1*, *siE6AP*, *pRK5-HA-Ubiquitin-K48R* (17604; Addgene), or an empty plasmid control using Attractene (Qiagen). After transfection for 2 days, the cells were collected for related experiments. To express the active-site cysteine-to-alanine mutant of E6AP in endothelial cells, *p3869HA-E6AP C833A* cells (8649; Addgene) were used. The C-A mutation was introduced at the site of E6AP C833 (22, 27). The *K48R mutant ubiquitin* was obtained from Dr. Guanghui Wang (Soochow University) (27). All the constructs were confirmed by sequencing.

#### Lentiviral vectors preparation for brain delivery

To construct a lentiviral vector expressing *Prx1*, two complementary *Prx1* DNA oligonucleotides were synthesized and inserted into the *EcoRI-BamHI* site of transfer vector *pCDH-CMV-MCS-EF1-copGFP* under the control of promoter *CMV*. The constructed vector was transformed into DH5a *Escherichia coli* and isolated with minipreps plasmid purification system (Promega). A large production of LV-*Prx1* was prepared by transfection of human kidney 293T cells. In brief, 293T cells were cotransfected with a mixture containing packaging plasmid (*pCD/NL-BH\*DDD*), envelope plasmid (*pLTR-G*), and transfer vector and Trans-EZ. For high-titer virus stocks, the supernatant of cells was collected at 72 h after transfection, low-speed centrifuged, filtered, and ultracentrifuged. The titer of LV-*Prx1* stock was determined by transduction of HOS cells with serial dilutions of concentrated lentivirus and analyzing integrated viral DNA copies per cell by quantitative polymerase chain reaction. The lentiviral vectors coding for *GFP* without *Prx1* were prepared in a similar manner, as described above, and used as a control (LV-*GFP*). In addition, we used a lentivirus-mediated RNA interference approach to achieve the inhibition of E6AP levels in the brain. The short hairpin RNA (shRNA)-mediated *Ube3a* knockdown vectors were constructed by subcloning the U6 promoter-sh-*Ube3a* cassette into the *AgeI-EcoRI* sites of the *pLenti-CMV* vector.

The lentiviral vector encoding mouse *Prx1* (LV-*GFP-Prx1*), LV-*GFP*, or sh-*E6AP* was injected into the right lateral ventricle over a 10-min duration using a Hamilton microsyringe with the coordinates of 0.5 mm caudal to the bregma, 1 mm lateral to the midline, and 3 mm depth from the skull surface under the guidance of a stereotaxic instrument. Two weeks after the introduction of the viral vectors, the MCAO mice model was prepared as previously reported (51). All lentivirus batches used for experiments had comparable titers ranging from  $1 \times 10^8$  to  $1 \times 10^9$  integration units/ml. Virus suspensions were stored at  $-80^\circ\text{C}$  until use and were briefly centrifuged and kept on ice immediately before injection.

#### RNA interference

*Prx1* siRNAs or *E6AP* siRNAs was introduced into EA.hy926 cells with the transfection medium according to

the manufacturer's instructions. The control set of EA.hy926 cells was transfected with nontargeted siRNAs. The cells were collected for experiments 72 h after transfection. Knockdown was confirmed with western blotting using whole cell lysates. *siPrx1* (sc-36177) and scramble negative control (sc-37007) were obtained from Santa Cruz Biotechnology: *siE6AP* (sense), 5'-GCCAGACACAGAAAGGUUTT-3'; scramble negative control (*siCont-1*, sense), 5'-UUGC GGGUCUAAUCACCGATT-3'.

#### Annexin V/PI flow cytometry analysis

Flow cytometric assays to evaluate apoptosis by Annexin V/PI (BioVision) staining were performed essentially as previously described, following the manufacturer's instruction. Briefly, endothelial cells were transfected with *Prx1* siRNAs for 48 h before exposure to 6 h OGD. Annexin V-FITC and PI were added to the cell suspension and incubated at room temperature for 10 min in the dark. For each sample, at least  $1 \times 10^4$  cells were analyzed using a FACS-Calibur flow cytometer (BD Biosciences).

#### TUNEL assay

*In situ* DNA fragmentation was assessed using a TUNEL staining combined with 4',6-diamidino-2-phenylindole (DAPI) counterstain. Images were recorded after counterstaining with DAPI (nuclei marker), and endothelial cells were identified by phase image. Endothelial cells were imaged using 20 $\times$  objectives. The apoptotic response was expressed as the percentage of TUNEL-positive endothelial cells/the total number of nuclei counted after DAPI staining. The results represented the average of a minimum of three experiments, and a minimum of 600 cells were counted per experiment.

#### Cell fractionation, immunoprecipitation, and immunoblotting analysis

Immunoblotting was carried out in endothelial cell lysates after determination of protein concentrations using the Bradford's solution. The cell lysates containing equivalent amounts of protein were applied to 10%–13.5% acrylamide denaturing gels (SDS-polyacrylamide gel electrophoresis [PAGE]) (15). Proteins were then transferred to an immobilon polyvinylidene difluoride membrane for 1 h at 50 V. Membranes were blocked in 20 mM Tris-HCl (PH 7.4), 150 mM NaCl, and 0.1% Tween 20 (TBS-T) containing 5% fat-free milk powder for 1 h and immunodetected with antibodies to HSP27 monoclonal antibody (1:1000), *Prx1* polyclonal antibody (1:5000), (Abcam); HO-1 (1:1000), Phospho-AKT (1:1000), Phospho-ERK (1:3000), Phospho-JNK (1:1000), Phospho-P38 (1:1000), Phospho-FKHR (1:3000), and cleaved Caspase-3 (1:1000, polyclonal antibody; Cell Signaling Technology); procaspase-3 (1:2000), PARP-1 (1:2000), and ubiquitin (1:1000, polyclonal antibody; Santa Cruz Biotechnology); ZO-1 and Occludin (1:1000; Invitrogen); E6AP (1:3000) and  $\beta$ -actin (1:5000, monoclonal antibody; Sigma-Aldrich). After incubation for 12 h, membranes were incubated with the appropriate horseradish peroxidase-conjugated secondary antibody. Immunoreactivity was visualized by enhanced chemiluminescence (Amersham Life Science). The *Prx1* ubiquitylation assays were performed essentially as described previously (46). Briefly, cells were treated with 5  $\mu\text{M}$  MG132 (Calbiochem)

or with dimethyl sulfoxide (DMSO; control) for 30 min before OGD. Immunoprecipitates were analyzed by immunoblotting, using either anti-ubiquitin or anti-Prx1 antibody to detect ubiquitylated Prx1. In addition, E6AP immunoprecipitates from the lysates were probed with anti-nitrotyrosine antibody.

#### Experimental animals

Male C57 mice, weighing 20–23 g, were obtained from the Zhejiang Medical Animal Centre (Hangzhou, China). Mice were housed under climate-controlled conditions with a 12-h light/dark cycle and provided with standard food and water. Animals were acclimated to their environment for at least 1 week before initiating the experimental protocols. All experimental protocols and animal handling procedures were performed in accordance with the National Institutes of Health (NIH) guidelines for the care and use of laboratory animals and were approved by the Committee for Animal Experiments at the Zhejiang University in China.

#### tMCAO model

The transient/reperfusion MCAO model was used to resemble stroke in humans (3, 5), and the surgery was carried out as previously described (18). Animal procedures were approved by the Committee on Animal Experiments at the Zhejiang University. The rectal temperature was monitored throughout the surgery, and the body temperature was maintained at  $37^{\circ}\text{C} \pm 0.5^{\circ}\text{C}$  with a heating pad. Neurological deficit tests were carried out at 24 h after tMCAO, including neurological scores and rotarod test. Neurological scores were determined 24 h after tMCAO using a previously described scoring system (45). Rotarod test, which started 3 days before the surgery to train five times every day, was performed to examine the motor coordination. The rotarod time (s) that mice persisted on the rotarod after ischemia was recorded; the data were expressed as the mean duration of five trials at 24 h after tMCAO. The brain infarct area of mice 24 h after ischemia was evaluated from scanned digital images of Nissl-stained brain sections using Image J software (NIH).

#### Evaluation of BBB damage

The loss of BBB integrity was also verified by the leakage of Texas red-conjugated dextran from microvessels after intravenous injection. Texas red-dextran (70 kDa) solution (0.1% in phosphate-buffered saline [PBS], 5 ml/kg) was intravenously administered *via* the tail vein at 22 h after the onset of MCAO. The mice were perfused transcardially with saline as above. After decapitation, brains were prepared according to the immunohistochemical methods, and Texas red-dextran leakage was determined by immunofluorescence staining (red fluorescence).

#### Confocal immunofluorescence staining and analysis

For immunofluorescence analysis in cultured endothelial cells, cells were fixed in 4% formaldehyde/PBS as previously reported (16). Cells were labeled with Prx1 (1:300, polyclonal antibody; Abcam), Nitrotyrosine (1:200, monoclonal antibody; Millipore), E6AP (1:300, polyclonal antibody; Invitrogen), and ubiquitin (1:200, monoclonal antibody; Cell Signaling Technology), followed by immunofluorescence using a standard protocol from PerkinElmer Life Sciences,

Inc. Nuclei were stained with DAPI dihydrochloride bis-benzimidazole (5  $\mu\text{M}$ ). Immunolocalization and changes in Prx1, E6AP, and nitrotyrosine in cultured endothelial cells were visualized by confocal microscopy (Zeiss LSM 510).

For immunohistochemistry, mice were anesthetized at the time of sacrifice and transcardially perfused with 4% paraformaldehyde in PBS as previously described (16). The whole brains were immediately removed and post-fixed overnight at  $4^{\circ}\text{C}$ . Then, brains were cut into 35- $\mu\text{m}$ -thick serial sections using a vibratome. Sections were incubated at room temperature in PBS with 0.01% Triton-X100 for 30 min and for 1 h in 3% bovine serum albumin (BSA) in PBS. For immunolabeling, the brain slices were incubated with antibodies targeting Prx1 (1:300; Abcam), CD31 (1:200; Santa Cruz Biotechnology), Claudin5 (1:200; Invitrogen), E6AP (1:300; Sigma-Aldrich), NeuN (1:300), and Nitrotyrosine (1:200) (Millipore) overnight at  $4^{\circ}\text{C}$ . After washing, the sections were incubated with Alexa fluor 488-conjugated anti-rabbit IgG (1:400) and Alexa fluor 594-conjugated anti-mouse IgG (1:400) (Invitrogen) in (Tris-NaCl-blocking) TNB buffer (1:400). In addition, the oxidative fluorescent indicator dihydroethidium was used to evaluate *in situ*  $\text{O}_2^{\bullet-}$  generation as previously reported (45). Immunofluorescence was visualized by using a Zeiss LSM 510 confocal microscope.

#### Statistical analysis

The data were analyzed with *t*-tests when means between two groups were compared. For multigroup comparisons, statistical significance was determined using one-way ANOVA followed by a *post hoc* Tukey's test or Dunnett's comparison to control. All data are expressed as the mean  $\pm$  SEM. A value of  $p < 0.05$  was considered to be significant.

#### Acknowledgments

This work was supported in part by the National Natural Science Foundation of China (81120108023, 91232705, 81202533); the Zhejiang Provincial Qianjiang Talent Plan (2012R10036); the Zhejiang Provincial Natural Science Foundation of China (R2100281); NIH grants (NHLBI HL-68686, NIDDK DK-49870, and DK-36079).

#### Author Disclosure Statement

No competing financial interests exist.

#### References

1. Aracena P, Tang W, Hamilton SL, and Hidalgo C. Effects of S-glutathionylation and S-nitrosylation on calmodulin binding to triads and FKBP12 binding to type 1 calcium release channels. *Antioxid Redox Signal* 7: 870–881, 2005.
2. Armulik A, Genové G, Mäe M, Nisancioglu MH, Wallgard E, Niaudet C, He L, Norlin J, Lindblom P, Strittmatter K, Johansson BR, and Betsholtz C. Pericytes regulate the blood-brain barrier. *Nature* 468: 557–561, 2010.
3. Braeuninger S and Kleinschnitz C. Rodent models of focal cerebral ischemia: procedural pitfalls and translational problems. *Exp Transl Stroke Med* 1: 8, 2009.
4. Brunet Simioni M, De Thonel A, Hammann A, Joly AL, Bossis G, Fourmaux E, Bouchot A, Landry J, Piechaczyk M, and Garrido C. Heat shock protein 27 is involved in SUMO-2/3 modification of heat shock factor 1 and thereby

- modulates the transcription factor activity. *Oncogene* 28: 3332–3344, 2009.
5. Carmichael ST. Rodent models of focal stroke: size, mechanism, and purpose. *NeuroRx* 2: 396–409, 2005.
  6. Chae HZ, Kang SW, and Rhee SG. Isoforms of mammalian peroxiredoxin that reduce peroxides in presence of thioredoxin. *Methods Enzymol* 300: 219–226, 1999.
  7. Chae HZ, Oubrahim H, Park JW, Rhee SG, and Chock PB. Protein glutathionylation in the regulation of peroxiredoxins: a family of thiol-specific peroxidases that function as antioxidants, molecular chaperones, and signal modulators. *Antioxid Redox Signal* 16: 506–523, 2012.
  8. Coe H, Bedard K, Groenendyk J, Jung J, and Michalak M. Endoplasmic reticulum stress in the absence of calnexin. *Cell Stress Chaperones* 13: 497–507, 2008.
  9. del Zoppo GJ. . The neurovascular unit, matrix proteases, and innate inflammation. *Ann N Y Acad Sci* 1207: 46–49, 2010.
  10. Fisher AB. Peroxiredoxin 6: a bifunctional enzyme with glutathione peroxidase and phospholipase A<sub>2</sub> activities. *Antioxid Redox Signal* 15: 831–844, 2011.
  11. Gan Y, Ji X, Hu X, Luo Y, Zhang L, Li P, Liu X, Yan F, Vosler P, Gao Y, Stetler RA, and Chen J. Transgenic overexpression of peroxiredoxin-2 attenuates ischemic neuronal injury via suppression of a redox-sensitive pro-death signaling pathway. *Antioxid Redox Signal* 17: 719–732, 2012.
  12. Geraerts M, Eggermont K, Hernandez-Acosta P, Garcia-Verdugo JM, Baekelandt V, and Debyser Z. Lentiviral vectors mediate efficient and stable gene transfer in adult neural stem cells *in vivo*. *Hum Gene Ther* 17: 635–650, 2006.
  13. Girouard H, Park L, Anrather J, Zhou P, and Iadecola C. Cerebrovascular nitrosative stress mediates neurovascular and endothelial dysfunction induced by angiotensin II. *Arterioscler Thromb Vasc Biol* 27: 303–309, 2007.
  14. Guo X, Yamada S, Tanimoto A, Ding Y, Wang KY, Shimajiri S, Murata Y, Kimura S, Tasaki T, Nabeshima A, Watanabe T, Kohno K, and Sasaguri Y. Overexpression of peroxiredoxin 4 attenuates atherosclerosis in apolipoprotein E knockout mice. *Antioxid Redox Signal* 17: 1362–1375, 2012.
  15. Han F, Ali Raie A, Shioda N, Qin ZH, and Fukunaga K. Accumulation of beta-amyloid in the brain microvessels accompanies increased hyperphosphorylated tau proteins following microsphere embolism in aged rats. *Neuroscience* 153: 414–427, 2008.
  16. Han F, Chen YX, Lu YM, Huang JY, Zhang GS, Tao RR, Ji YL, Liao MH, Fukunaga K, and Qin ZH. Regulation of the ischemia-induced autophagy-lysosome processes by nitrosative stress in endothelial cells. *J Pineal Res* 51: 124–135, 2011.
  17. Han F, Shirasaki Y, and Fukunaga K. Microsphere embolism-induced endothelial nitric oxide synthase expression mediates disruption of the blood-brain barrier in rat brain. *J Neurochem* 99: 97–106, 2006.
  18. Han F, Tao RR, Zhang GS, Lu YM, Liu LL, Chen YX, Lou YJ, Fukunaga K, and Hong ZH. Melatonin ameliorates ischemic-like injury-evoked nitrosative stress: Involvement of HtrA2/PED pathways in endothelial cells. *J Pineal Res* 50: 281–291, 2011.
  19. Hu BR, Martone ME, Jones YZ, and Liu CL. Protein aggregation following transient cerebral ischemia. *J Neurosci* 20: 3191–3199, 2000.
  20. Jakobsson J and Lundberg C. Lentiviral vectors for use in the central nervous system. *Mol Ther* 13: 484–493, 2006.
  21. Kakihana T, Nagata K, and Sitia R. Peroxides and peroxidases in the endoplasmic reticulum: integrating redox homeostasis and oxidative folding. *Antioxid Redox Signal* 16: 763–771, 2012.
  22. Kao WH, Beaudenon SL, Talis AL, Huibregtse JM, and Howley PM. Human papillomavirus type 16 E6 induces self-ubiquitination of the E6AP ubiquitin-protein ligase. *J Virol* 74: 6408–6417, 2000.
  23. Kim SY, Kim TJ, and Lee KY. A novel function of peroxiredoxin 1 (Prx-1) in apoptosis signal-regulating kinase 1 (ASK1)-mediated signaling pathway. *FEBS Lett* 582: 1913–1918, 2008.
  24. Kim YJ, Ahn JY, Liang P, Ip C, Zhang Y, and Park YM. Human prx1 gene is a target of Nrf2 and is upregulated by hypoxia/reoxygenation: implication to tumor biology. *Cancer Res* 67: 546–554, 2007.
  25. Kisucka J, Chauhan AK, Patten IS, Yesilaltay A, Neumann C, Van Etten RA, Krieger M, and Wagner DD. Peroxiredoxin1 prevents excessive endothelial activation and early atherosclerosis. *Circ Res* 103: 598–605, 2008.
  26. Leblanc GG, Golanov E, Awad IA, and Young WL. Biology of Vascular Malformations of the Brain NINDS Workshop Collaborators. Biology of vascular malformations of the brain. *Stroke* 40: e694–e702, 2009.
  27. Liu C, Fei E, Wang H, Tao R, Iwata A, Nukina N, Zhou J, and Wang G. Assembly of lysine 63-linked ubiquitin conjugates by phosphorylated-synuclein implies lewy body biogenesis. *J Biol Chem* 282: 14558–14566, 2007.
  28. Liu G, Feinstein SI, Wang Y, Dodia C, Fisher D, Yu K, Ho YS, and Fisher AB. Comparison of glutathione peroxidase 1 and peroxiredoxin 6 in protection against oxidative stress in the mouse lung. *Free Radic Biol Med* 49: 1172–1181, 2010.
  29. Liu QB, Liu LL, Lu YM, Tao RR, Huang JY, Han F, and Lou YJ. The induction of reactive oxygen species and loss of mitochondrial Omi/HtrA2 is associated with S-nitrosoglutathione-induced apoptosis in human endothelial cells. *Toxicol Appl Pharmacol* 244: 374–384, 2010.
  30. Manczak M, Mao P, Calkins MJ, Cornea A, Reddy AP, Murphy MP, Szeto HH, Park B, and Reddy PH. Mitochondria-targeted antioxidants protect against amyloid-beta toxicity in Alzheimer's disease neurons. *J Alzheimers Dis* 20: S609–S631, 2010.
  31. Mowbray AL, Kang DH, Rhee SG, Kang SW, and Jo H. Laminar shear stress up-regulates peroxiredoxins (PRX) in endothelial cells: PRX 1 as a mechanosensitive antioxidant. *J Biol Chem* 283: 1622–1627, 2008.
  32. Nakamura T and Lipton SA. S-nitrosylation of critical protein thiols mediates protein misfolding and mitochondrial dysfunction in neurodegenerative diseases. *Antioxid Redox Signal* 14: 1479–1492, 2011.
  33. Nasu J, Murakami K, Miyagawa S, Yamashita R, Ichimura T, Wakita T, Hotta H, Miyamura T, Suzuki T, Satoh T, and Shoji I. E6AP ubiquitin ligase mediates ubiquitin-dependent degradation of peroxiredoxin 1. *J Cell Biochem* 111: 676–685, 2010.
  34. Neumann CA, Krause DS, Carman CV, Das S, Dubey DP, Abraham JL, Bronson RT, Fujiwara Y, Orkin SH, and Van Etten RA. Essential role for the peroxiredoxin Prdx1 in erythrocyte antioxidant defence and tumour suppression. *Nature* 424: 561–565, 2003.
  35. Pitts A, Dailey K, Newington JT, Chien A, Arseneault R, Cann T, Thompson LM, and Cumming RC. Dithiol based compounds maintain expression of antioxidant protein

- peroxiredoxin 1 that counteracts toxicity of mutant hungtinton. *J Biol Chem* 287: 22717–22729, 2012.
36. Quaegebeur A, Segura I, and Carmeliet P. Pericytes: blood-brain barrier safeguards against neurodegeneration? *Neuron* 68: 321–323, 2010.
  37. Quaegebeur A, Lange C, and Carmeliet P. The neurovascular link in health and disease: molecular mechanisms and therapeutic implications. *Neuron* 71: 406–424, 2011.
  38. Rabilloud T, Heller M, Gasnier F, Luche S, Rey C, Aebbersold R, Benahmed M, Louisot P, and Lunardi J. Proteomics analysis of cellular response to oxidative stress. Evidence for *in vivo* overoxidation of peroxiredoxins at their active site. *J Biol Chem* 277: 19396–19401, 2002.
  39. Rani V, Neumann CA, Shao C, and Tischfield JA. Prdx1 deficiency in mice promotes tissue specific loss of heterozygosity mediated by deficiency in DNA repair and increased oxidative stress. *Mutat Res* 735: 39–45, 2012.
  40. Riddell JR, Maier P, Sass SN, Moser MT, Foster BA, and Gollnick SO. Peroxiredoxin 1 stimulates endothelial cell expression of VEGF *via* TLR4 dependent activation of HIF-1 $\alpha$ . *PLoS One* 7: e50394, 2012.
  41. Rizzo MT and Leaver HA. Brain endothelial cell death: modes, signaling pathways, and relevance to neural development, homeostasis, and disease. *Mol Neurobiol* 42: 52–63, 2010.
  42. Rott R, Szargel R, Haskin J, Bandopadhyay R, Lees AJ, Shani V, and Engelender S.  $\alpha$ -Synuclein fate is determined by USP9X-regulated monoubiquitination. *Proc Natl Acad Sci U S A* 108: 18666–186671, 2011.
  43. Satoh M, Fujimoto S, Haruna Y, Arakawa S, Horike H, Komai N, Sasaki T, Tsuboi K, Makino H, and Kashihara N. NAD(P)H oxidase and uncoupled nitric oxide synthase are major sources of glomerular superoxide in rats with experimental diabetic nephropathy. *Am J Physiol Renal Physiol* 288: F1144–F1152, 2005.
  44. Schreiber G, van Horssen J, Haseloff RF, Reijerkerk A, van der Pol SM, Nieuwenhuizen O, Krause E, Blasig IE, Dijkstra CD, Ronken E, and de Vries HE. Protective effects of peroxiredoxin-1 at the injured blood-brain barrier. *Free Radic Biol Med* 45: 256–264, 2008.
  45. Shioda N, Han F, Moriguchi S, and Fukunaga K. Constitutively active calcineurin mediates delayed neuronal death through Fas-ligand expression *via* activation of NFAT and FKHR transcriptional activities in mouse brain ischemia. *J Neurochem* 102: 1506–1517, 2007.
  46. Shirakura M, Murakami K, Ichimura T, Suzuki R, Shimoji T, Fukuda K, Abe K, Sato S, Fukasawa M, Yamakawa Y, Nishijima M, Moriishi K, Matsuura Y, Wakita T, Suzuki T, Howley PM, Miyamura T, and Shoji I. E6AP ubiquitin ligase mediates ubiquitylation and degradation of hepatitis C virus core protein. *J Virol* 81: 1174–1185, 2007.
  47. Sultana R, Perluigi M, Newman SF, Pierce WM, Cini C, Coccia R, and Butterfield DA. Redox proteomic analysis of carbonylated brain proteins in mild cognitive impairment and early Alzheimer's disease. *Antioxid Redox Signal* 12: 327–336, 2010.
  48. Tan KH, Harrington S, Purcell WM, and Hurst RD. Peroxynitrite mediates nitric oxide-induced blood-brain barrier damage. *Neurochem Res* 29: 579–587, 2004.
  49. Tao RR, Ji YL, Lu YM, Fukunaga K, and Han F. Targeting nitrosative stress for neurovascular protection: new implications in brain diseases. *Curr Drug Targets* 13: 272–284, 2012.
  50. Wilcox CS and Pearlman A. Chemistry and antihypertensive effects of tempol and other nitroxides. *Pharmacol Rev* 60: 418–469, 2008.
  51. Zhang GS, Tian Y, Huang JY, Tao RR, Liao MH, Lu YM, Ye WF, Wang R, Fukunaga K, Lou YJ, and Han F. The  $\gamma$ -Secretase blocker DAPT reduces the permeability of the blood-brain barrier by decreasing the ubiquitination and degradation of occludin during permanent brain ischemia. *CNS Neurosci Ther* 19: 53–60, 2012.

Address correspondence to:

Dr. Feng Han  
Institute of Pharmacology, Toxicology  
and Biochemical Pharmaceutics  
Zhejiang University  
Hangzhou 310058  
China

E-mail: changhuahan@zju.edu.cn

Date of first submission to ARS Central, April 18, 2013; date of final revised submission, November 12, 2013; date of acceptance, December 2, 2013.

#### Abbreviations Used

ASK1 = apoptosis signal-regulating kinase 1
BBB = blood-brain barrier
DAPI = 4',6-diamidino-2-phenylindole
DMEM = Dulbecco's modified Eagle's medium
E6AP = E6-associated protein
ER = endoplasmic reticulum
FKHR = forkhead transcription factor Foxo1
H <sub>2</sub> O <sub>2</sub> = hydrogen peroxide
HBMEC = human brain microvascular endothelial cell
HO-1 = heme oxygenase-1
HSP27 = heat shock protein 27
JNK = c-Jun N-terminal kinase
MALDI-TOF = matrix-assisted laser desorption/ionization-time-of-flight
mHtt = mutant Hungtinton
MMPs = metalloproteinases
NeuN = neuronal nuclear marker
NO = nitric oxide
Nrf2 = NF-E2-related factor 2
O <sub>2</sub> <sup>•-</sup> = superoxide
OGD = oxygen-glucose deprivation
ONOO <sup>-</sup> = peroxynitrite
PAGE = polyacrylamide gel electrophoresis
PARP = poly ADP-ribose polymerase
PBS = phosphate-buffered saline
PI = propidium iodide
Prx = peroxiredoxin
ROS = reactive oxygen species
SDS = sodium dodecyl sulfate
shRNA = short hairpin RNA
SIN-1 = 3-morpholiniosydnonimine
siRNA = small interfering RNA
tMCAO = transient middle cerebral artery occlusion
TUNEL = terminal deoxynucleotidyl transferase dUTP nick end labeling
ZO-1 = zonula occludens-1